



ELSEVIER

Available online at www.sciencedirect.com

SCIENCE @ DIRECT®

Nuclear Physics B 663 [FS] (2003) 409–442

NUCLEAR
PHYSICS B

www.elsevier.com/locate/npe

Critical RSOS and minimal models: fermionic paths, Virasoro algebra and fields

Giovanni Feverati, Paul A. Pearce

Department of Mathematics and Statistics, University of Melbourne, Parkville, Victoria 3010, Australia

Received 27 November 2002; received in revised form 21 March 2003; accepted 25 April 2003

Abstract

A framework is presented to extend the finitized characters and recursion methods of (off-critical) corner transfer matrices (CTMs), in a self-consistent fashion, to the calculation of CFT characters and conformal partition functions. More specifically, in this paper we consider $s\ell(2)$ minimal conformal field theories on a cylinder from a lattice perspective. We argue that a general energy-preserving bijection exists between the one-dimensional configuration paths of the A_L restricted solid-on-solid (RSOS) lattice models and the eigenstates of their double row transfer matrices and exhibit this bijection for the critical and tricritical Ising models in the vacuum sector. To each allowed one-dimensional configuration path we associate a physical state and a monomial in a finite fermionic algebra. The orthonormal states produced by the action of these monomials on the primary states $|h\rangle$ generate finite Virasoro modules with dimensions given by the finitized Virasoro characters $\chi_h^{(N)}(q)$. These finitized characters are the generating functions for the double row transfer matrix spectra of the critical RSOS models. We also propose a general level-by-level algorithm to build matrix representations of the Virasoro generators and chiral vertex operators (CVOs). The algorithm employs a distinguished basis which we call the L_1 -basis. Our results extend to \mathbb{Z}_{L-1} parafermion models by duality.

© 2003 Elsevier B.V. All rights reserved.

PACS: 11.25.Hf; 05.50.+q; 05.70.Jk; 75.10.Hk

1. Introduction

Over the last two decades there has been much progress in understanding the deep connections between conformal field theory (CFT) [1,2] and integrable lattice models [3]

E-mail addresses: feverati@ms.unimelb.edu.au (G. Feverati), p.pearce@ms.unimelb.edu.au (P.A. Pearce).

0550-3213/03/\$ – see front matter © 2003 Elsevier B.V. All rights reserved.

doi:10.1016/S0550-3213(03)00375-4

but some intriguing mysteries remain. Within the framework of Baxter’s corner transfer matrices (CTMs), for example, it is well known that the one-dimensional configuration sums generate conformal characters in the thermodynamic limit. But conceptually this is not well understood. For the fundamental example of the solvable ABF models [4], the one-dimensional configuration sums are

$$X_{abc}^{(N)}(q) = \sum_{\{\sigma\}} q^{H(\sigma_{j-1}, \sigma_j, \sigma_{j+1})}, \quad \sigma_0 = a, \quad \sigma_N = b, \quad \sigma_{N+1} = c, \quad (1.1)$$

where $H(\sigma_{j-1}, \sigma_j, \sigma_{j+1}) = \frac{1}{2}|\sigma_{j-1} - \sigma_{j+1}|$ is a local energy and the sum is over all paths $\sigma = \{\sigma_0, \sigma_1, \dots, \sigma_{N+1}\}$ with $\sigma_j \in \{1, 2, \dots, L\}$ and $\sigma_j - \sigma_{j+1} = \pm 1$. In the thermodynamic limit these one-dimensional configuration sums *formally* yield the $s\ell(2)$ minimal Virasoro characters

$$q^{c/24 - h_{r,s}} \chi_{r,s}(q) = \lim_{N \rightarrow \infty} X_{s,r,r+1}^{(N)}(q). \quad (1.2)$$

Baxter’s celebrated CTM formalism [3] was originally proposed as a method to calculate local one-point functions for off-critical solvable lattice models. But with its appealing description of the character generating functions in terms of a local energy along paths, the one-dimensional configuration sums have also proved to be a useful tool within CFT for studying characters. In particular, they provide natural finitizations of the characters as well as mathematically powerful recursion relations between the finitized characters. These have played an important role, for example, in the study of the fermionic forms [5] of various characters which have led to many recent developments [6,7]. From the CFT point of view, however, the CTM formalism suffers from certain shortcomings and inherent inconsistencies. First, the formalism is limited to special boundary conditions (dictated by off-critical groundstates) and does not extend to periodic and other conformal boundary conditions. Second, the CTMs refer to off-critical lattice models which do not exhibit conformal symmetry. Moreover, an appropriate Yang–Baxter integrable off-critical regime that correctly reproduces the characters may not even exist. In the case of the ABF models, both regimes III and IV are adjacent to the relevant critical line but only the regime III one-dimensional configuration sums correctly yield the Virasoro characters [8,9]. But even more serious is the fact that, in the off-critical lattice models, the parameter q is the elliptic nome measuring the departure-from-criticality which is entirely unrelated to any modular parameter q . Consequently, there is no relation between the *formally identified* parameters q appearing on the left- and right-hand sides of the key relation (1.2) which embodies the *correspondence principle* of the Kyoto school [8].

In this paper we remove these shortcomings and inconsistencies by building on work [10] on a fermionic interpretation of Baxter’s corner transfer matrix (CTM) paths. In the context of the $s\ell(2)$ minimal models, we show that the same paths, the same local energy, the same finitized characters and the same recursion relations can all be obtained, in a self-consistent fashion, by working with *critical* double-row transfer matrices with modular parameter

$$q = \exp\left(-\pi \sin(Lu) \frac{M}{N}\right), \quad (1.3)$$

where M/N is the lattice aspect ratio and u is the spectral parameter. Our lattice approach naturally leads us to take steps towards a fermionization of the minimal CFTs. In its present form our formalism is somewhat cumbersome and we do not suggest it should replace the usual bosonic Coulomb gas methods for practical calculations. However, since the minimal models (with the exception of the Ising model) do not contain fermionic fields, we feel that the existence of a consistent fermionization is significant especially in the light of the known fermionic forms for the characters.

The layout of this paper is as follows. In Section 2, we define the critical RSOS models and their double-row transfer matrices. We also recall their relation to the minimal and parafermion CFTs. The bijection between the one-dimensional RSOS configuration paths and eigenstates of the critical RSOS double row transfer matrices is exhibited for the critical and tricritical Ising models in Section 3. In Section 4, we introduce fermionic algebras. We give the relation between physical states and fermionic paths and discuss fermionic states and finite Virasoro modules. As a by-product of our considerations we present in Section 5 a general level-by-level algorithm to build explicit matrix representations of the Virasoro generators and chiral vertex operators (CVOs) in a basis of fermionic paths. These concrete matrix representations will be useful in further developing a lattice approach to studying CFT. We conclude in Section 7 with a discussion of open questions for further research. An expanded version of this work containing more examples of building matrix representations for the critical Ising, tricritical Ising, 3-state Potts and Yang–Lee theories on a cylinder can be found on the archives [11].

2. Critical RSOS models and conformal field theory

2.1. Critical RSOS models and double row transfer matrices

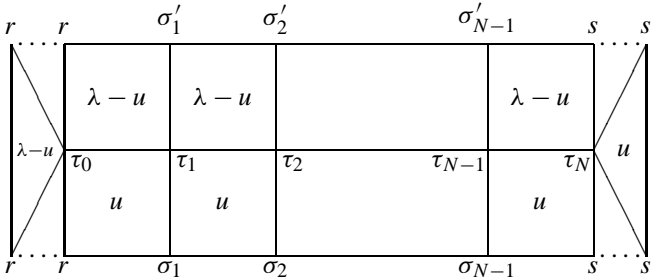
The critical A_L RSOS models [4] are exactly solvable models [3] on the square lattice. The Boltzmann weights associated to the elementary faces are

$$W \left(\begin{array}{cc} d & c \\ a & b \end{array} \middle| u \right) = \begin{array}{c} d \\ \square \\ a \end{array} \begin{array}{c} c \\ u \\ b \end{array} = \frac{\sin(\lambda - u)}{\sin \lambda} \delta_{a,c} + \frac{\sin u}{\sin \lambda} \sqrt{\frac{S_a S_c}{S_b S_d}} \delta_{b,d}, \tag{2.1}$$

where the heights $a, b, c, d \in \{1, 2, \dots, L\}$ and u is the spectral parameter. The crossing parameter is $\lambda = \frac{(p-p')\pi}{p}$ with p, p' coprime and $p' < p = L + 1$. The crossing factors are $S_a = \sin a\lambda$ and the weights vanish if the heights on any edge do not differ by ± 1 . For *unitary* models ($p' = p - 1$), these Boltzmann weights are all nonnegative whereas, for *nonunitary* models ($p' < p - 1$), some of these weights are negative.

Since the RSOS face weights satisfy the Yang–Baxter equation (YBE), these models are integrable for arbitrary complex u using commuting transfer matrix methods [3]. To work on a strip or cylinder, with specified boundary conditions (r_L, s_L) on the left and (r_R, s_R) on the right edges, it is necessary to introduce [12] double row transfer matrices. In this paper we will consider just the subset of boundary conditions with $(r_L, s_L) = (r, 1)$ and $(r_R, s_R) = (1, s)$. We call these (r, s) type boundary conditions. With (r, s) boundary

conditions, the double row transfer matrices are represented diagrammatically by

$$\mathbf{D}(u)_{\sigma, \sigma'} = \sum_{\tau_0, \dots, \tau_N}$$


(2.2)

For integrability, the triangle boundary weights on the left and right must satisfy the boundary Yang–Baxter equation (BYBE). For each conformal boundary condition (r_L, s_L) or (r_R, s_R) on an edge, there is a corresponding integrable boundary condition [13] given by a set of triangle boundary weights satisfying the BYBE. For (r, s) type boundary conditions, the partition functions satisfy $Z_{(1,1)|(r,s)} = Z_{(r,1)|(1,s)}$. In the vacuum sector $(r_L, s_L) = (r_R, s_R) = (1, 1)$, the triangle boundary weights vanish unless $\tau_0 = \tau_N = 2$ so the triangle boundary weights can simply be removed leaving the heights alternating between 1 and 2 on the left and right edges of the strip.

For boundary conditions of (r, s) type, the double row transfer matrices $\mathbf{D}(u)$ form a commuting family $[\mathbf{D}(u), \mathbf{D}(v)] = 0$. Consequently, they can be simultaneously diagonalized by the orthogonal matrix of eigenstates which are independent of u . For a suitable choice of parameters, the double row transfer matrices are real symmetric and positive definite. The actual form of the eigenstates changes under an orthogonal change of basis. Nevertheless, these eigenstates are characterized by their associated eigenvalues $D(u)$ which are independent of the choice of basis. These eigenvalues in turn can be studied analytically by Yang–Baxter techniques and are classified according to their patterns of zeros in the complex u -plane. Consequently, we can use the patterns of zeros to label the eigenstates.

The A_L RSOS models exhibit two distinct physical regimes. If $0 < u < \lambda$, the continuum scaling limit realizes the $s\ell(2)$ minimal models. Otherwise, if $\lambda - \pi/2 < u < 0$, the continuum scaling limit realizes the \mathbb{Z}_{L-1} parafermions. The conformal data is obtained from the finite-size corrections to the eigenvalues of the double row transfer matrices. In making contact with CFT, the spectral parameter is usually specialized to its isotropic value, $u = \lambda/2$ for minimal models and $u = -\lambda$ for \mathbb{Z}_{L-1} parafermions.

2.2. Minimal models and \mathbb{Z}_k parafermions

The $s\ell(2)$ minimal models [1] $\mathcal{M}(p', p)$ with p, p' coprime have central charges

$$c = 1 - \frac{6(p - p')^2}{pp'} \tag{2.3}$$

The conformal weights are

$$h = h_{r,s} = \frac{(rp - sp')^2 - (p - p')^2}{4pp'}, \quad r = 1, 2, \dots, p' - 1; \quad s = 1, 2, \dots, p - 1 \tag{2.4}$$

and the Virasoro characters are

$$\chi_h(q) = \frac{q^{-c/24+h}}{(q)_\infty} \sum_{k=-\infty}^{\infty} (q^{k(kpp'+rp-sp')} - q^{(kp+s)(kp'+r)}), \tag{2.5}$$

where

$$(q)_n = \prod_{k=1}^n (1 - q^k). \tag{2.6}$$

The minimal models are unitary if $p - p' = \pm 1$. We consider only the diagonal A -type series with $p' < p$. The critical Ising $\mathcal{M}(3, 4)$, tricritical Ising $\mathcal{M}(4, 5)$ and Yang–Lee theories $\mathcal{M}(2, 5)$ are the prototypical examples.

The $s\ell(2) \mathbb{Z}_k$ parafermion models [14] have central charges

$$c = \frac{2(k - 1)}{k + 2}, \quad k = 2, 3, \dots \tag{2.7}$$

We consider only the diagonal A -type series. The \mathbb{Z}_3 or hard hexagon model [3,15] is the prototypical example. The hard hexagon model is in the universality class of the 3-state Potts model so we refer to this as the 3-state Potts CFT. Generally, the characters of the \mathbb{Z}_k models are string functions but, for the \mathbb{Z}_3 model, these are easily related to the Virasoro characters of the $\mathcal{M}(5, 6)$ model.

The minimal and \mathbb{Z}_k parafermion models are rational and admit a finite number of primary fields $\phi(z) = \phi^{(h)}(z)$. These theories arise from the continuum scaling limit of the A_L RSOS models with $L = p - 1$ and $L = k + 1$, respectively.

2.3. Virasoro algebra and Virasoro states

The Virasoro algebra

$$\text{Vir} = \langle L_n, n \in \mathbb{Z} \rangle \tag{2.8}$$

is an infinite-dimensional complex Lie algebra associated with conformal symmetry. The generators L_n satisfy the commutation relations

$$[L_n, L_m] = (n - m)L_{n+m} + \frac{c}{12}n(n^2 - 1)\delta_{n,-m}, \tag{2.9}$$

where the central element c is the central charge. The Virasoro generators are the modes of the energy–momentum tensor

$$T(z) = \sum_{n \in \mathbb{Z}} L_n z^{-n-2}. \tag{2.10}$$

On a cylinder with prescribed boundary conditions, which is the case of primary concern here, there is just one copy of the Virasoro algebra. For bulk theories on the torus, however, there is a second copy $\overline{\text{Vir}}$ of Virasoro which is the antiholomorphic counterpart.

For rational CFTs, the Hilbert space \mathcal{H} of states on which Vir acts is naturally decomposed into a finite direct sum of irreducible highest weight representations (Virasoro modules)

$$\mathcal{H} = \bigoplus_h \mathcal{V}_h, \tag{2.11}$$

where the sum is over the conformal weights h of the primary fields $\phi(z) = \phi^{(h)}(z)$. The vacuum $|0\rangle$ and primary (highest weight) states $|h\rangle$ are characterized by

$$L_0|h\rangle = h|h\rangle, \quad L_n|0\rangle = 0, \quad n \geq -1; \quad L_n|h\rangle = 0, \quad n > 0. \tag{2.12}$$

Moreover, there is a one-to-one correspondence between primary fields and primary states induced by

$$\lim_{z \rightarrow 0} \phi^{(h)}(z)|0\rangle = |h\rangle. \tag{2.13}$$

The vacuum state $|0\rangle$ with $h = 0$ corresponds to the identity operator.

The generically reducible highest weight representation of Vir (Verma module) is the linear span of Virasoro states in the canonical form

$$L_{-n_j} L_{-n_{j-1}} \cdots L_{-n_1} |h\rangle, \quad n_j \geq n_{j-1} \geq \cdots \geq n_1 \geq 1. \tag{2.14}$$

If its maximal proper submodule is quotiented out, we are led to the irreducible Virasoro module $\mathcal{V}_h = \mathcal{V}_{c,h}$ and the states (2.14) are no longer linearly independent due to the existence of null vectors. The generic Virasoro module in the $h = 0$ vacuum sector is shown in Fig. 1. Typically, for given c and h , some states at a given level enter in a vanishing non-trivial linear combination that is the null vector. Surprisingly, it seems that a complete set of linearly independent Virasoro states is not known even for the Ising model, although it is known [16] for the Yang–Lee theory $\mathcal{M}(2, 5)$ and the whole family $\mathcal{M}(2, 2n + 3)$, $n \geq 1$.

With reference to the vectors (2.14), the module \mathcal{V}_h is graded according to the level

$$\mathcal{V}_h = \bigoplus_{\ell=0}^{\infty} \mathcal{V}_{h,\ell}, \quad \ell = \sum_{i=1}^j n_i. \tag{2.15}$$

The Virasoro character $\chi_h(q)$, which is the generating function for the spectrum of the Virasoro module \mathcal{V}_h , is

$$\chi_h(q) = \text{Tr}_{\mathcal{V}_h} q^{L_0 - c/24} = q^{-c/24+h} \sum_{\ell=0}^{\infty} d_\ell q^\ell, \quad d_\ell \geq 0, \tag{2.16}$$

where q is the modular parameter and the degeneracy $d_\ell = d_\ell^h = \dim \mathcal{V}_{h,\ell}$ is the dimension of the space of states at level ℓ .

1	0⟩			
0	–			
q^2	$L_{-2} 0⟩$			
q^3	$L_{-3} 0⟩$			
$2q^4$	$L_{-4} 0⟩$	$L_{-2}^2 0⟩$		
$2q^5$	$L_{-5} 0⟩$	$L_{-3}L_{-2} 0⟩$		
$4q^6$	$L_{-6} 0⟩$	$L_{-4}L_{-2} 0⟩$	$L_{-3}^2 0⟩$	$L_{-2}^3 0⟩$
$4q^7$	$L_{-7} 0⟩$	$L_{-5}L_{-2} 0⟩$	$L_{-4}L_{-3} 0⟩$	$L_{-3}L_{-2}^2 0⟩$
$7q^8$	$L_{-8} 0⟩$	$L_{-6}L_{-2} 0⟩$	$L_{-5}L_{-3} 0⟩$	$L_{-4}^2 0⟩$
	$L_{-4}L_{-2}^2 0⟩$	$L_{-3}^2L_{-2} 0⟩$	$L_{-2}^4 0⟩$	
$8q^9$
$12q^{10}$

Fig. 1. Virasoro module \mathcal{V}_0 of Virasoro states in the vacuum $h = 0$ sector. The generic Virasoro character is $\chi_0(q) = \prod_{n=2}^{\infty} (1 - q^n)^{-1} = 1 + q^2 + q^3 + 2q^4 + 2q^5 + 4q^6 + 4q^7 + 7q^8 + 8q^9 + 12q^{10} + \dots$. In this sector, there is a null vector $L_{-1}|0\rangle = 0$ at level $\ell = 1$. For the minimal theories $\mathcal{M}(p', p)$, further null vectors appear. For example, for the Ising model $\mathcal{M}(3, 4)$, there is one null vector at level 6 and 7 and two at level 8. For $\mathcal{M}(4, 5)$, the first null vector enters at level 12.

3. Bijections of paths and strings

In this section we discuss the bijection between the fermionic paths and eigenstates of the critical RSOS double row transfer matrices. More specifically, we exhibit an energy preserving bijection between the RSOS paths and patterns of zeros classifying the eigenvalues of the double row transfer matrices. We use the work of Warnaar [10] to further establish a bijection with fermionic particles. Although they are equi-numerous, the fermionic RSOS paths that label the eigenstates of the transfer matrices are not the same as the RSOS paths on which the transfer matrices act. These states can only be related by a complicated orthogonal transformation. It also needs to be emphasized that our bijection is between the fermionic RSOS paths and the patterns of zeros of the eigenvalues of the double row transfer matrices $D(u)$. Within the framework of the usual Bethe ansatz, a separate bijection exists [17] between the RSOS paths and the rigged configurations related to the patterns of zeros of Baxter’s auxiliary matrix $Q(u)$.

Although we assert that our bijections are general, we content ourselves here with illustrating the bijections in the vacuum $h = 0$ sectors of the unitary minimal models. In these cases the classification of eigenstates of the double row transfer matrices and their accompanying patterns of zeros are completely known [18] in terms of (m, n) -systems [9, 19]. The full details of the bijections for the unitary minimal models in all (r, s) sectors and with periodic boundary conditions will be given elsewhere [20]. In the case of periodic boundaries, there are two copies of the Virasoro algebra and the states are labeled by two RSOS paths. In the plane of the complex spectral parameter u , these come from the distinct patterns of zeros in the upper and lower half-planes corresponding respectively to the left- and right-chiral halves. On the cylinder, the complex conjugation symmetry ensures that the patterns of zeros in the upper and lower half-planes are the same so there is only one RSOS path and one copy of the Virasoro algebra.

3.1. One-dimensional configuration sums

Consider the N -step configuration paths $\{\sigma\}$ of the A_L RSOS models [4] as shown in Figs. 2 and 3 with $\sigma_j \in \{1, 2, 3, \dots, L\}$ and $\sigma_{j+1} - \sigma_j = \pm 1$. In this context, applying conformal boundary conditions of (r, s) type means that $\sigma_0 = s, \sigma_N = r$ and $\sigma_{N+1} = r + 1$ where $s = 1, 2, \dots, L$ and $r = 1, 2, \dots, L - 1$. Alternatively, we can work with infinite paths which start at s and after N steps alternate between heights r and $r + 1$. Allowing for the \mathbb{Z}_2 height reversal symmetry, there are $\frac{1}{2}L(L - 1)$ distinct boundary conditions or sectors. In the case of the unitary minimal models $\mathcal{M}(L, L + 1)$, these are in one-to-one

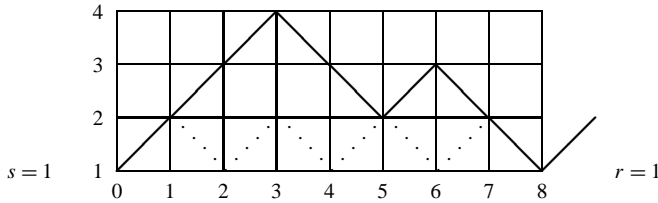


Fig. 2. The $N = 8$ step RSOS configurational path $\sigma = \{1, 2, 3, 4, 3, 2, 3, 2, 1\}$ in the vacuum $(r, s) = (1, 1)$ sector of the tricritical Ising model $\mathcal{M}(4, 5)$. The energy of this path is $E(\sigma) = \frac{1}{2}(1 + 2 + 4 + 7) = 7$. The groundstate vacuum path $|0\rangle$ is shown dotted.

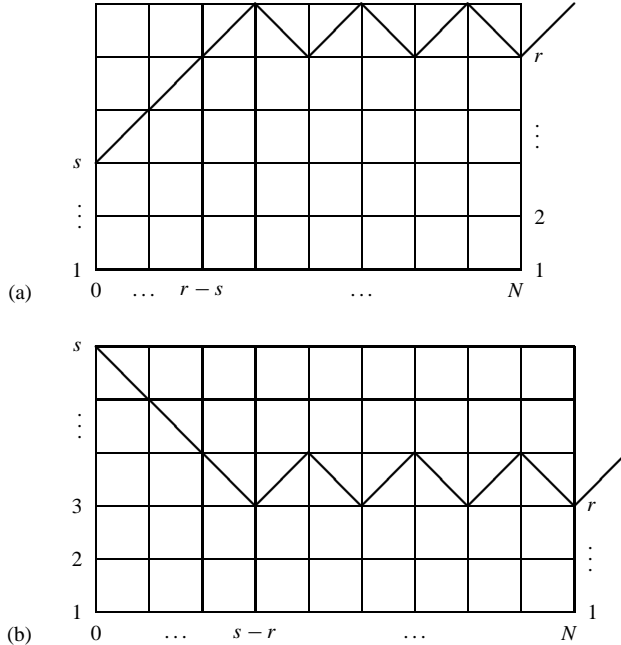


Fig. 3. The N -step path σ_h associated with the primary state $|h\rangle$ of the (r, s) sector for (a) $s \leq r$ and (b) $s > r$. The parity of N is fixed by $N = |r - s| \bmod 2$. Sectors of type (a) and (b) are related by the \mathbb{Z}_2 Kac table symmetry $(r, s) \equiv (L - r, L + 1 - s)$ under height reversal.

correspondence with the primary operators $\phi^{(h)}(z)$ with conformal weights in the Kac table

$$h = h_{r,s} = h_{L-r,L+1-s} = \frac{((L+1)r - Ls)^2 - 1}{4L(L+1)}, \quad 1 \leq r \leq L-1, \quad 1 \leq s \leq L. \tag{3.1}$$

These RSOS paths were first introduced in the context of the corner transfer matrices (CTMs) for the off-critical RSOS models but here we use these same paths at criticality to classify the eigenstates of the critical RSOS double row transfer matrices. Each path is associated with a state $|\sigma\rangle$ with configurational energy

$$E(\sigma) = \frac{1}{2} \sum_{j=1}^N j H(\sigma_{j-1}, \sigma_j, \sigma_{j+1}). \tag{3.2}$$

For the unitary minimal models $\mathcal{M}(L, L+1)$ the elementary local excitation energy is

$$H(\sigma_{j-1}, \sigma_j, \sigma_{j+1}) = \frac{1}{2} |\sigma_{j-1} - \sigma_{j+1}| = \begin{cases} 0, & \sigma_{j+1} = \sigma_{j-1}, \\ 1, & \sigma_{j+1} - \sigma_{j-1} = \pm 2. \end{cases} \tag{3.3}$$

This description originates with the off-critical RSOS models in regime III with q the elliptic modulus but here we apply it to the regime III/IV critical RSOS models with q the modular parameter. The vacuum or groundstate $|0\rangle$ with zero energy is the path that alternates between heights 1 and 2. In the (r, s) sector, the primary or reference state $|h\rangle$ is the path σ_h with lowest energy as shown in Fig. 3. The (r, s) sector is associated with the Virasoro module \mathcal{V}_h with $h = h_{r,s}$. Specifically, the finitized Virasoro characters $\chi_{r,s}^{(N)}(q) = \chi_h^{(N)}(q)$ approach the corresponding Virasoro characters in the limit $N \rightarrow \infty$ with $N = |r - s| \bmod 2$

$$\chi_h^{(N)}(q) := q^{-c/24+h} \sum_{\{\sigma\}} q^{E(\sigma) - E(\sigma_h)} \rightarrow \chi_h(q), \quad N \rightarrow \infty. \tag{3.4}$$

3.2. Critical Ising model

The central charge of the critical Ising $\mathcal{M}(3, 4)$ model is $c = 1/2$. Let us consider the vacuum sector with boundary condition $(r, s) = (1, 1)$ and $h = 0$. The excitation energies are given by the scaling limit of the eigenvalues $D(u)$ of the double-row transfer matrix $D(u)$. The eigenvalues $D(u)$ are classified [18] according to their zeros in the complex u -plane falling in or on the boundary of the single analyticity strip

$$-\frac{\lambda}{2} < \text{Re}(u) < \frac{3\lambda}{2}, \tag{3.5}$$

where $\lambda = \pi/4$ is the crossing parameter. For finite N , the low lying excitations contain 1-strings (zeros in the middle of the strip) and 2-strings (pairs of zeros at the edges of the strip with the same imaginary part). By complex conjugation symmetry, the patterns of zeros in the upper and lower half-planes are the same so we only consider the upper half-plane. It is found that if the number of 1-strings in the upper half-plane is m and the

number of 2-strings is n then this string content satisfies the simple (m, n) -system

$$m + n = \frac{N}{2}, \tag{3.6}$$

where m and N are even.

The lowest or groundstate energy $E = 0$ occurs for $m = 0$. Among excitations with given string content, the lowest energy $E = m^2/2$ occurs when all of the 1-strings are further from the real axis than all of the 2-strings. Moreover, for given string content, it is found that all patterns of zeros obtained by permuting the vertical positions of the 1- and 2-strings actually occur among the eigenvalues. Each time the position of adjacent 1- and 2-strings is interchanged the energy is increased by one unit. It follows [18] that the spectrum generating function is given by the finitized character

$$\begin{aligned} \chi_0^{(N)}(q) &= q^{-c/24} \sum_E q^E = q^{-c/24} \sum_{m=0,2,4,\dots} q^{m^2/2} \left[\begin{matrix} N/2 \\ m \end{matrix} \right]_q \\ &\rightarrow q^{-c/24} \sum_{m=0,2,4,\dots} \frac{q^{m^2/2}}{(q)_m} = \chi_0(q), \end{aligned} \tag{3.7}$$

where the q -binomials are

$$\left[\begin{matrix} m+n \\ m \end{matrix} \right]_q = \begin{cases} \frac{(q)_{m+n}}{(q)_m(q)_n}, & m, n \geq 0, \\ 0, & \text{otherwise} \end{cases} \tag{3.8}$$

with $(q)_n$ given by (2.6) and $(q)_0 = 1$.

3.3. Tricritical Ising model

The central charge of the tricritical Ising $\mathcal{M}(4, 5)$ model is $c = 7/10$. Again let us consider the vacuum sector with boundary condition $(r, s) = (1, 1)$ and $h = 0$. In classifying [18] the eigenvalues $D(u)$ of the double-row transfer matrix $\mathbf{D}(u)$ there are now two relevant analyticity strips in the complex u -plane

$$(1) \quad -\frac{\lambda}{2} < \text{Re}(u) < \frac{3\lambda}{2}, \quad (2) \quad 2\lambda < \text{Re}(u) < 4\lambda, \tag{3.9}$$

where the crossing parameter is $\lambda = \pi/5$. The excitations are again classified by the string content in the upper half u -plane

$$\begin{aligned} m_i &= \{\text{number of 1-strings in strip } i = 1, 2\}, \\ n_i &= \{\text{number of 2-strings in strip } i = 1, 2\}, \end{aligned} \tag{3.10}$$

where m_1, m_2 and N are even and satisfy the (\mathbf{m}, \mathbf{n}) system

$$m_1 + n_1 = \frac{N + m_2}{2}, \quad m_2 + n_2 = \frac{m_1}{2}. \tag{3.11}$$

The groundstate energy $E = 0$ now corresponds to $m_1 = m_2 = 0$. For excitations with given string content (\mathbf{m}, \mathbf{n}) , the lowest energy $E = (m_1^2 - m_1 m_2 + m_2^2)/2$ occurs when,

in both strips 1 and 2, all of the 1-strings are further out from the real axis than all of the 2-strings in the strip. Bringing the location of a 1-string, in either strip 1 or 2, closer to the real axis by interchanging its location with an adjacent 2-string increments the excitation energy E by one unit. It thus follows [18] that the spectrum generating function is given by the finitized character

$$\begin{aligned} \chi_0^{(N)}(q) &= q^{-c/24} \sum_{m_1, m_2=0,2,4,\dots} q^{(m_1^2 - m_1 m_2 + m_2^2)/2} \begin{bmatrix} (N + m_2)/2 \\ m_1 \end{bmatrix}_q \begin{bmatrix} m_1/2 \\ m_2 \end{bmatrix}_q \\ &\rightarrow q^{-c/24} \sum_{m_1, m_2=0,2,4,\dots} \frac{q^{(m_1^2 - m_1 m_2 + m_2^2)/2}}{(q)_{m_1}} \begin{bmatrix} m_1/2 \\ m_2 \end{bmatrix}_q = \chi_0(q). \end{aligned} \tag{3.12}$$

3.4. Unitary minimal models

The critical and tricritical Ising models are the first two in the A_L series of unitary minimal models $\mathcal{M}(L, L + 1)$. Again considering the $(r, s) = (1, 1)$ vacuum sector with $h = 0$, the eigenvalues of the double row transfer matrices can be classified [20] by the number of 1-strings m_i and the number of 2-strings n_i in $L - 2$ analyticity strips. These must satisfy the (\mathbf{m}, \mathbf{n}) system [9,19]

$$\mathbf{m} + \mathbf{n} = \frac{1}{2}(N\mathbf{e}_1 + A\mathbf{m}), \tag{3.13}$$

where A is the adjacency matrix of A_{L-2} , $C = 2I - A$ is the Cartan matrix and $\mathbf{e}_1 = (1, 0, \dots, 0)$. Here \mathbf{m}, \mathbf{n} and \mathbf{e}_1 are $(L - 2)$ -dimensional vectors and each m_i and N must be even. The finitized characters, generalizing (3.7) and (3.12), are [9,19]

$$\begin{aligned} \chi_0^{(N)}(q) &= q^{-c/24} \sum_{(\mathbf{m}, \mathbf{n})} q^{\frac{1}{4}\mathbf{m}C\mathbf{m}} \prod_{i=1}^{L-2} \begin{bmatrix} m_i + n_i \\ m_i \end{bmatrix}_q \\ &\rightarrow q^{-c/24} \sum_{m_i=0,2,4,\dots} \frac{q^{\frac{1}{4}\mathbf{m}C\mathbf{m}}}{(q)_{m_1}} \prod_{i=2}^{L-2} \begin{bmatrix} m_i + n_i \\ m_i \end{bmatrix}_q = \chi_0(q). \end{aligned} \tag{3.14}$$

These finite characters agree precisely with the finitized characters (3.4) and they reproduce the correct counting of states with $q = 1$. The limiting forms of these characters, however, differ fundamentally from (2.5) because the coefficients in the q -series (3.7), (3.12) and (3.14) are manifestly nonnegative. For this reason these forms are called *fermionic* [5] in contrast to the *bosonic* form (2.5).

3.5. Energy-preserving bijection

Since the energy spectrum generating functions for the paths and strings coincide, it is natural to expect an energy-preserving bijection between the two descriptions of the states. Given an RSOS path, Warnaar [10] has given a detailed prescription to extract the fermionic particle content. There are $L - 1$ types of particles. A particle of type i at position j corresponds to a peak in the RSOS path at height i above the baseline as shown in Fig. 4.

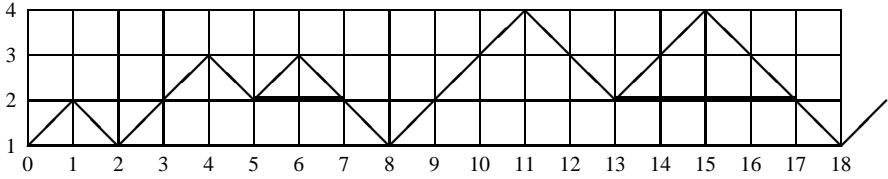


Fig. 4. A typical A_4 RSOS path of $N = 18$ steps decomposed into a series of overlapping peaks by drawing in a sequence of horizontal baselines following the prescription of Warnaar [10]. This prescription reveals particles of type 1, 2, 1, 3, 2 at positions $j = 1, 4, 6, 11, 15$ respectively and a particle content $n_1 = 2, n_2 = 2, n_3 = 1$. A particle of type i has a peak i units above the baseline and a width (at the baseline) of $2i$.

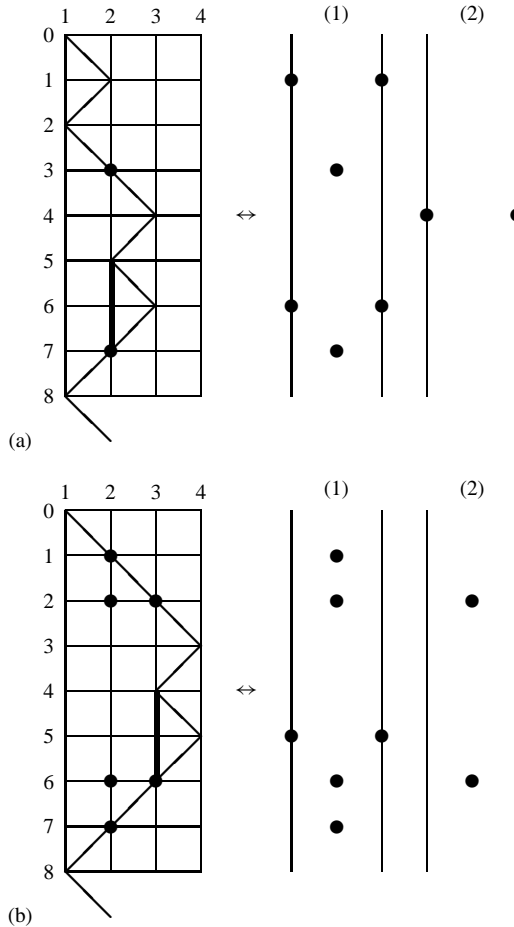


Fig. 5. Bijection of tricritical Ising RSOS paths and strings. The RSOS paths (rotated 90° clockwise) are shown on the left and the strips (1) and (2) containing 1- and 2-strings in the upper-half complex u -plane are shown on the right. The string (particle) content is (a) $m_1 = 2, n_1 = 2, m_2 = 0, n_2 = 1, n_3 = 0$, (b) $m_1 = 4, n_1 = 1, m_2 = 2, n_2 = 0, n_3 = 1$.

For $1 \leq i \leq L - 2$, this corresponds to a 2-string in strip i at position j . Consequently, the number of particles n_i of type i coincides with the n_i of the (\mathbf{m}, \mathbf{n}) system for $i \leq L - 2$. Since the width of a particle of type i is $2i$, the particle number n_{L-1} is simply determined by the constraint

$$\sum_{i=1}^{L-1} 2in_i = N. \tag{3.15}$$

The m_i are interpreted as the number of dual-particles of type i for $1 \leq i \leq L - 2$. In an RSOS path, a dual-particle of type i at position j corresponds to a domain wall (straight segment with $H(\sigma_{j-1}, \sigma_j, \sigma_{j+1}) = 1$) at height i above the baseline. In turn, this corresponds to 1-strings at position j in strips 1 through i . We remark that in the string description the absolute position of the strings in a strip is of no importance, only the relative ordering of 1- and 2-strings in each strip is pertinent. The rules of this bijection are illustrated in Fig. 5 for two typical RSOS paths of the A_4 tricritical Ising model. In the case of the $\mathcal{M}(L, L + 1)$ models the bijection works the same but there are $L - 2$ such strips each containing 1- and 2-strings.

4. Fermionic algebras and states

4.1. Fermionic algebras

Let us just consider the RSOS models related to unitary minimal models in the sector $h = h_{r,s}$. Then at each position j along an A_L path σ there is either a corner with energy 0 or a straight segment with energy 1 and these two possibilities are mutually exclusive. We regard an elementary excitation as the action of a fermionic operator $b_{\mp j/2} = b_{\mp j/2}^\dagger$ that annihilates (creates) a corner at position j of σ and creates (annihilates) a straight segment at the same position of σ . The fermionic behavior (Pauli exclusion principle) is suggested by the fact that at position j only one straight segment or corner can exist

$$b_{\pm j/2}^2 = 0. \tag{4.1}$$

The associated energy $H(\sigma_{j-1}, \sigma_j, \sigma_{j+1})$ is the eigenvalue of the fermion number operator

$$b_{-j/2} b_{j/2} |\sigma\rangle = H(\sigma_{j-1}, \sigma_j, \sigma_{j+1}) |\sigma\rangle, \tag{4.2}$$

where in anticipation of unitarity we have set $b_{j/2} = b_{-j/2}^\dagger$.

The dual description originates with the RSOS models in the off-critical regime II but here we apply it to the critical regime I/II RSOS models describing \mathbb{Z}_{L-1} parafermions. In the dual description the roles of the corners and straight segments are interchanged so that

$$H'(\sigma_{j-1}, \sigma_j, \sigma_{j+1}) = 1 - H(\sigma_{j-1}, \sigma_j, \sigma_{j+1}) = \begin{cases} 0, & \sigma_{j+1} - \sigma_{j-1} = \pm 2, \\ 1, & \sigma_{j+1} = \sigma_{j-1}. \end{cases} \tag{4.3}$$

Apart from a shift in the zero of energy, this involves an overall change of sign in the energy $E(\sigma)$. The groundstate $|0\rangle'$ with zero energy is now the saw-tooth path (see Fig. 7) $\sigma = \{1, 2, \dots, L - 1, L, L - 1, \dots, 2, 1, 2, \dots\}$. In this dual picture an elementary excitation annihilates a straight segment and creates a corner at position j of the path. The associated energy $H'(\sigma_{j-1}, \sigma_j, \sigma_{j+1})$ is the eigenvalue of the dual fermion number operator

$$b_{\frac{j}{2}} b_{-\frac{j}{2}} |\sigma\rangle = H'(\sigma_{j-1}, \sigma_j, \sigma_{j+1}) |\sigma\rangle. \tag{4.4}$$

Comparison with (3.3) and (4.3) suggests that

$$b_{-\frac{j}{2}} b_{\frac{j}{2}} + b_{\frac{j}{2}} b_{-\frac{j}{2}} = 1 \tag{4.5}$$

consistent with our fermionic interpretation. Guided by the Ising or free fermion $\mathcal{M}(3, 4)$ case, we assume the additional fermionic relations $b_j b_k = -b_k b_j, j \neq -k$.

We now introduce a fermionic algebra generated by all the fermion operators

$$\mathcal{F} = \bigoplus_h \mathcal{F}_h, \quad \mathcal{F}_h = \langle b_j^h, j \in \mathbb{Z}/2, j \neq 0 \rangle. \tag{4.6}$$

There is an independent copy \mathcal{F}_h of the fermion algebra in each sector h with

$$b_j^h b_k^{h'} = b_j^h b_k^h \delta_{h,h'}. \tag{4.7}$$

We usually work in a fixed sector and suppress the index h . The generators in each sector satisfy the usual canonical anticommutation relations (CAR) for fermions as well as the involutive property for real fermions

$$\{b_j, b_k\} = \delta_{j,-k}, \quad b_{-j} = b_j^\dagger = b_j^T. \tag{4.8}$$

The fermion number operators $b_{-j} b_j$ are mutually commuting projectors

$$\begin{aligned} (b_{-j} b_j)^2 &= b_{-j} b_j; & [b_{-j} b_j, b_{-k} b_k] &= 0, \quad j, k \neq 0; \\ [b_{-j} b_j, b_k] &= 0, \quad j \neq \pm k. \end{aligned} \tag{4.9}$$

On the lattice this algebra is *finitized* by setting

$$b_{\frac{j}{2}} = 0, \quad |j| > N. \tag{4.10}$$

This yields a closed finite-dimensional fermionic algebra

$$\mathcal{F}^{(N)} = \bigoplus_h \mathcal{F}_h^{(N)}, \quad \mathcal{F}_h^{(N)} = \left\langle b_j^h, j = \pm \frac{1}{2}, \pm 1, \dots, \pm \frac{N}{2} \right\rangle. \tag{4.11}$$

A matrix representation of the fermionic algebra $\mathcal{F}_h^{(N)}$ is easily obtained in terms of $2^N \times 2^N$ real matrices with entries $0, \pm 1$. The dimension of this algebra is 2^N since at each position there can be a straight segment or a corner (4.1), that is, at each position a monomial in the basis can contain a $b_{-j/2}$ or the identity 1.

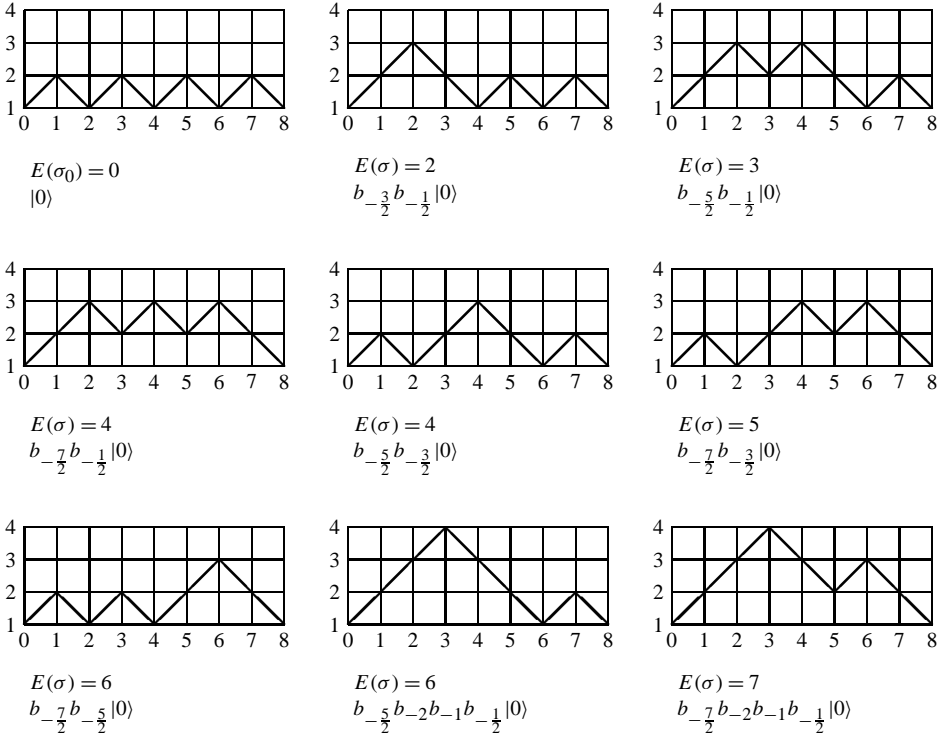


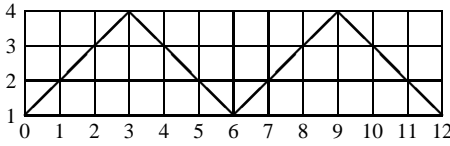
Fig. 6. The first few RSOS configurational paths for the vacuum sector $\mathcal{V}_0^{(8)}$ of $\mathcal{M}(4, 5)$ with energy given by (3.3). These states are also listed in Fig. 9. The rule (4.1) associates physical fermionic states with paths.

Each allowed path is naturally associated with a fermionic monomial (see Figs. 6 and 7)

$$\{\sigma\}_{j_1, j_2, j_3, \dots, j_n} \leftrightarrow b_{\mp \frac{j_n}{2}} \cdots b_{\mp \frac{j_2}{2}} b_{\mp \frac{j_2}{2}} b_{\mp \frac{j_1}{2}} \in \mathcal{F}_h, \quad j_n > \cdots > j_3 > j_2 > j_1 > 0 \tag{4.12}$$

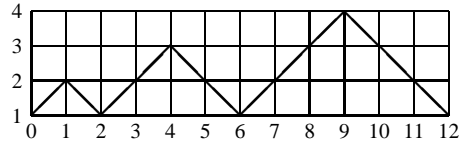
(anticommutation of the fermion operators has been used to bring them into canonical order) according to the following rules as in (4.1):

- The path σ_h corresponding to the primary state $|h\rangle$ is associated to the identity in the fermionic algebra \mathcal{F}_h .
- At each position j where a corner of the primary state path is changed to a straight line we put a creation operator $b_{-\frac{j}{2}}$ and at each position j where a straight line of the primary state path is changed to a corner we put an annihilation operator $b_{\frac{j}{2}}$.
- No operators are inserted when a corner or straight line is unchanged.



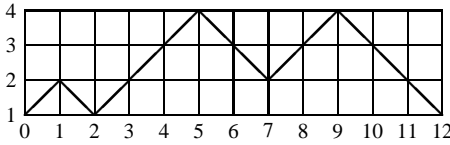
$$E(\sigma) - E(\sigma_0) = 0$$

$$|0\rangle$$



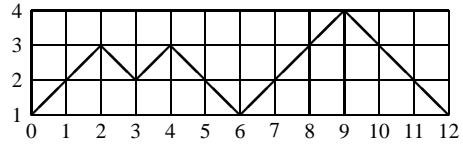
$$E(\sigma) - E(\sigma_0) = 2$$

$$b_2 b_{-\frac{3}{2}} b_1 b_{\frac{1}{2}} |0\rangle$$



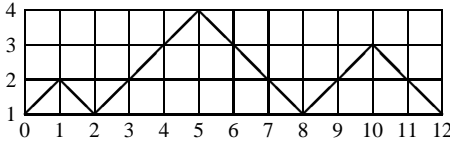
$$E(\sigma) - E(\sigma_0) = 3$$

$$b_7 b_{-3} b_5 b_{-\frac{3}{2}} b_1 b_{\frac{1}{2}} |0\rangle$$



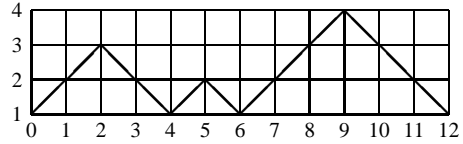
$$E(\sigma) - E(\sigma_0) = 3$$

$$b_2 b_1 |0\rangle$$



$$E(\sigma) - E(\sigma_0) = 4$$

$$b_5 b_{-\frac{9}{2}} b_4 b_{-3} b_5 b_{-\frac{3}{2}} b_1 b_{\frac{1}{2}} |0\rangle$$



$$E(\sigma) - E(\sigma_0) = 4$$

$$b_5 b_2 b_{-\frac{3}{2}} b_1 |0\rangle$$

Fig. 7. The first few RSOS configurational paths in the parafermionic \mathbb{Z}_3 vacuum sector $\mathcal{V}_0 \oplus \mathcal{V}_3$ of the 3-state Potts model with energy given by (4.3). The energy of the vacuum path (top-left corner) $\sigma_0 = \{1, 2, 3, 4, 3, 2, 1, 2, 3, 4, 3, 2, 1\}$ has been subtracted. We used the usual association rule (4.1) and ordered the b operators as they are obtained from the paths. The canonical order can be obtained by the anticommutation rules.

We call such a monomial a *physical monomial*. Among other constraints, the path restrictions imply

$$b_{-j} b_{-j-1/2} b_{-j-1} \cdots b_{-j-(L-2)/2} = \{\text{unphysical}\} \tag{4.13}$$

so that such combinations, which go beyond the heights of A_L and do not correspond to allowed paths, should never enter in the expressions of physical quantities and must be projected out.

Note that the product of two physical monomials need not be a physical monomial. As an example, consider the two physical monomials and associated A_4 paths

$$b_{-\frac{5}{2}} b_{-2} b_{-1} b_{-\frac{1}{2}} \leftrightarrow \{1, 2, 3, 4, 3, 2, 1, 2, 1\},$$

$$b_{-\frac{7}{2}} b_{-\frac{3}{2}} \leftrightarrow \{1, 2, 1, 2, 3, 2, 3, 2, 1\}.$$

1	0⟩			
0	–			
q^2	$b_{-\frac{3}{2}}b_{-\frac{1}{2}} 0⟩$			
q^3	$b_{-\frac{5}{2}}b_{-\frac{1}{2}} 0⟩$			
$2q^4$	$b_{-\frac{7}{2}}b_{-\frac{1}{2}} 0⟩$	$b_{-\frac{5}{2}}b_{-\frac{3}{2}} 0⟩$		
$2q^5$	$b_{-\frac{9}{2}}b_{-\frac{1}{2}} 0⟩$	$b_{-\frac{7}{2}}b_{-\frac{3}{2}} 0⟩$		
$4q^6$	$b_{-\frac{11}{2}}b_{-\frac{1}{2}} 0⟩$	$b_{-\frac{9}{2}}b_{-\frac{3}{2}} 0⟩$	$b_{-\frac{7}{2}}b_{-\frac{5}{2}} 0⟩$	$b_{-\frac{5}{2}}b_{-2}b_{-1}b_{-\frac{1}{2}} 0⟩$
$4q^7$	$b_{-\frac{13}{2}}b_{-\frac{1}{2}} 0⟩$	$b_{-\frac{11}{2}}b_{-\frac{3}{2}} 0⟩$	$b_{-\frac{9}{2}}b_{-\frac{5}{2}} 0⟩$	$b_{-\frac{7}{2}}b_{-2}b_{-1}b_{-\frac{1}{2}} 0⟩$
$7q^8$	$b_{-\frac{15}{2}}b_{-\frac{1}{2}} 0⟩$	$b_{-\frac{13}{2}}b_{-\frac{3}{2}} 0⟩$	$b_{-\frac{11}{2}}b_{-\frac{5}{2}} 0⟩$	$b_{-\frac{9}{2}}b_{-\frac{7}{2}} 0⟩$
	$b_{-\frac{7}{2}}b_{-\frac{5}{2}}b_{-\frac{3}{2}}b_{-\frac{1}{2}} 0⟩$	$b_{-\frac{9}{2}}b_{-2}b_{-1}b_{-\frac{1}{2}} 0⟩$	$b_{-\frac{7}{2}}b_{-3}b_{-1}b_{-\frac{1}{2}} 0⟩$	
$8q^9$
$12q^{10}$

Fig. 8. Generic Virasoro module \mathcal{V}_0 of orthonormal fermionic states in the $h = 0$ vacuum sector. The Virasoro character is $\chi_0(q) = \prod_{n=2}^{\infty} (1 - q^n)^{-1} = 1 + q^2 + q^3 + 2q^4 + 2q^5 + 4q^6 + 4q^7 + 7q^8 + 8q^9 + 12q^{10} + \dots$. The first few states, such as, $b_{-\frac{3}{2}}b_{-\frac{1}{2}}|0\rangle = \sqrt{\frac{2}{c}}L_{-2}|0\rangle$, $b_{-\frac{5}{2}}b_{-\frac{1}{2}}|0\rangle = \frac{1}{\sqrt{2c}}L_{-3}|0\rangle$, are easily related to Virasoro states. For finite p , unphysical (null) vectors appear. For example, for the Ising model $\mathcal{M}(3, 4)$, $b_{-\frac{5}{2}}b_{-2}b_{-1}b_{-\frac{1}{2}}|0\rangle$, $b_{-\frac{7}{2}}b_{-2}b_{-1}b_{-\frac{1}{2}}|0\rangle$, $b_{-\frac{9}{2}}b_{-2}b_{-1}b_{-\frac{1}{2}}|0\rangle$, $b_{-\frac{7}{2}}b_{-3}b_{-1}b_{-\frac{1}{2}}|0\rangle$ are null vectors. For $\mathcal{M}(4, 5)$, the first null vector enters at level 12.

We see that the product does not correspond to any A_4 path

$$(b_{-\frac{5}{2}}b_{-2}b_{-1}b_{-\frac{1}{2}})(b_{-\frac{7}{2}}b_{-\frac{3}{2}}) = b_{-\frac{7}{2}}b_{-\frac{5}{2}}b_{-2}b_{-\frac{3}{2}}b_{-1}b_{-\frac{1}{2}}. \tag{4.14}$$

4.2. Physical fermionic states, finite Virasoro modules and projectors

The identification (4.12) between physical fermionic monomials and paths can be used to define physical fermionic states

$$|\sigma\rangle = b_{\mp \frac{j_n}{2}} \cdots b_{\mp \frac{j_3}{2}} b_{\mp \frac{j_2}{2}} b_{\mp \frac{j_1}{2}} |h\rangle, \quad j_n > \cdots > j_3 > j_2 > j_1 > 0. \tag{4.15}$$

In the alternative view of infinite paths, the paths associated with these states must agree with the primary state $|h\rangle$ for all $j > N$ for some finite N . Normalizing the primary states so that $\langle h|h\rangle = 1$, it is easy to verify that the states (4.15) are orthonormal using the fermion algebra. Some physical fermionic states of $\mathcal{M}(4, 5)$ and the 3-state Potts model are shown in Figs. 6–9. A consequence of our definition of the primary state $|h\rangle$ is that it is annihilated by certain modes

$$\begin{aligned} b_{\frac{j}{2}}|h\rangle &= 0, & \text{if } \{\sigma_n\}_j \text{ is a corner,} \\ b_{-\frac{j}{2}}|h\rangle &= 0, & \text{if } \{\sigma_n\}_j \text{ is a straight line.} \end{aligned} \tag{4.16}$$

$$\begin{array}{ll}
 1 & |0\rangle \\
 0 & - \\
 q^2 & b_{-\frac{3}{2}} b_{-\frac{1}{2}} |0\rangle \\
 q^3 & b_{-\frac{5}{2}} b_{-\frac{1}{2}} |0\rangle \\
 2q^4 & b_{-\frac{7}{2}} b_{-\frac{1}{2}} |0\rangle \qquad b_{-\frac{5}{2}} b_{-\frac{3}{2}} |0\rangle \\
 q^5 & b_{-\frac{7}{2}} b_{-\frac{3}{2}} |0\rangle \\
 2q^6 & b_{-\frac{7}{2}} b_{-\frac{5}{2}} |0\rangle \qquad b_{-\frac{5}{2}} b_{-2} b_{-1} b_{-\frac{1}{2}} |0\rangle \\
 q^7 & b_{-\frac{7}{2}} b_{-2} b_{-1} b_{-\frac{1}{2}} |0\rangle \\
 2q^8 & b_{-\frac{7}{2}} b_{-\frac{5}{2}} b_{-\frac{3}{2}} b_{-\frac{1}{2}} |0\rangle \qquad b_{-\frac{7}{2}} b_{-3} b_{-1} b_{-\frac{1}{2}} |0\rangle \\
 q^9 & b_{-\frac{7}{2}} b_{-3} b_{-2} b_{-\frac{1}{2}} |0\rangle \\
 q^{10} & b_{-\frac{7}{2}} b_{-3} b_{-2} b_{-\frac{3}{2}} |0\rangle
 \end{array}$$

Fig. 9. Finite Virasoro module $\mathcal{V}_0^{(8)}$ of fermionic states in the vacuum $h = 0$ sector of $\mathcal{M}(4, 5)$. For $N = 8$ just 13 states survive after setting $b_j = 0$ for $|j| \geq 4$. The finitized character is $\chi_{1,1}^{(8)}(q) = 1 + q^2 + q^3 + 2q^4 + q^5 + 2q^6 + q^7 + 2q^8 + q^9 + q^{10}$.

We identify the linear span of physical fermionic states with the Virasoro module \mathcal{V}_h . The set of states (4.15) thus forms a fermionic basis \mathcal{B}_h for \mathcal{V}_h . The Hilbert space of physical states decomposes into a direct sum of modules

$$\mathcal{H} = \bigoplus_h \mathcal{V}_h \tag{4.17}$$

with fermionic basis $\mathcal{B} = \bigcup_h \mathcal{B}_h$. Again this space is graded according to the level

$$\mathcal{V}_h = \bigoplus_{\ell} \mathcal{V}_{h,\ell}, \quad \ell = \sum_{k=1}^n \frac{j_k}{2} - E(\sigma_h) = E(\sigma) - E(\sigma_h). \tag{4.18}$$

A generic Virasoro module of fermionic states in the $h = 0$ vacuum sector is shown in Fig. 8.

On the lattice, the *finitized* physical Hilbert space is

$$\mathcal{H}^{(N)} = \bigoplus_h \mathcal{V}_h^{(N)}, \tag{4.19}$$

where the *finite Virasoro module* $\mathcal{V}_h^{(N)}$ is the linear span of physical fermion states associated with N -step paths in the (r, s) sector. The number of independent physical fermion states forming the basis $\mathcal{B}_h^{(N)}$ of $\mathcal{V}_h^{(N)}$ is thus equal to the number of paths from height s to height r in N steps so that

$$\dim \mathcal{V}_h^{(N)} = |\mathcal{B}_h^{(N)}| = [A^N]_{r,s}, \tag{4.20}$$

where A is the adjacency matrix of A_L . The finite Virasoro module $\mathcal{V}_0^{(8)}$ of the $h = 0$ vacuum sector of $\mathcal{M}(4, 5)$ is shown in Fig. 6.

The projectors onto the physical states in \mathcal{H} and \mathcal{V}_h are given by complete sums over the fermionic basis of states

$$\mathcal{P} = \sum_{|\sigma\rangle \in \mathcal{B}} |\sigma\rangle\langle\sigma|, \quad \mathcal{P}_h = \sum_{|\sigma\rangle \in \mathcal{B}_h} |\sigma\rangle\langle\sigma|. \tag{4.21}$$

Consequently a physical operator ϕ on \mathcal{H} is determined by its matrix elements between physical states

$$\phi = \mathcal{P}\phi\mathcal{P} = \sum_{|\sigma\rangle, |\sigma'\rangle \in \mathcal{B}} \langle\sigma|\phi|\sigma'\rangle |\sigma\rangle\langle\sigma'|. \tag{4.22}$$

The elementary projectors are easily written in terms of fermions. For example, if $h = h_{3,1}$,

$$|0\rangle\langle 0| = \prod_{j=1}^{\infty} (1 - b_{-\frac{j}{2}}^0 b_{\frac{j}{2}}^0) \in \mathcal{F},$$

$$|h\rangle\langle h| = (b_{-\frac{1}{2}}^h b_{\frac{1}{2}}^h) (b_{-1}^h b_1^h) \prod_{j=3}^{\infty} (1 - b_{-\frac{j}{2}}^h b_{\frac{j}{2}}^h) \in \mathcal{F}. \tag{4.23}$$

It follows that the operator ϕ can be written entirely in terms of fermions once the matrix elements are known relative to a given fermionic basis. The algebra of physical observables is thus the subalgebra of the fermionic algebra \mathcal{F} obtained by projection

$$\mathcal{A} = \mathcal{P}\mathcal{F}\mathcal{P}. \tag{4.24}$$

Since the structure of this algebra is complicated, however, it is often easier to work in the larger unphysical fermion algebra \mathcal{F} and then project.

4.3. Hamiltonian and characters

The Hamiltonian of the fermionic system associated with the unitary minimal models in the (r, s) sector is

$$L_0 = \mathcal{P}_h \left(\sum_{j=1}^{\infty} \frac{j}{2} b_{-\frac{j}{2}} b_{\frac{j}{2}} - E(\sigma_h) + h \right) \mathcal{P}_h, \tag{4.25}$$

where \mathcal{P}_h is the projector onto physical states. We assert that each physical fermion state (4.15) is an eigenstate of the Hamiltonian (4.25) with eigenenergy given precisely by (3.2). Indeed, using the fermionic algebra we find

$$L_0|\sigma\rangle = L_0 b_{-\frac{j_1}{2}} b_{-\frac{j_2}{2}} \cdots b_{-\frac{j_n}{2}} |h\rangle = (E(\sigma) - E(\sigma_h) + h) b_{-\frac{j_1}{2}} b_{-\frac{j_2}{2}} \cdots b_{-\frac{j_n}{2}} |h\rangle, \tag{4.26}$$

where

$$E(\sigma) = \frac{1}{2} \sum_{j=1}^N j H(\sigma_{j-1}, \sigma_j, \sigma_{j+1}) = \sum_{k=1}^n \frac{j_k}{2}. \tag{4.27}$$

The Virasoro character which is the generating function for the spectrum of the Virasoro module is now

$$\chi_h(q) = q^{-c/24} \text{Tr}_{\mathcal{V}_h} q^{L_0}. \tag{4.28}$$

The finitized characters, given by the finitization $b_{\frac{j}{2}} = 0$ for $|j| > N$, are

$$\chi_h^{(N)}(q) = q^{-c/24} \text{Tr}_{\mathcal{V}_h^{(N)}} q^{L_0}. \tag{4.29}$$

These are the generating functions for the spectra of the finite Virasoro modules.

5. Algorithm for building matrix representations

In this section we present a general algorithm for building, level by level, matrix representations of the Virasoro generators and primary fields based on paths [16,21,22]. These concrete matrix representations will be useful in further developing a lattice approach to studying CFT. We will work in a distinguished orthonormal basis which we call the L_1 -basis. The algorithm itself relates the vectors of the L_1 -basis to the basis of Virasoro states (2.14). Applying the algorithm for generic c also yields general expressions for the null vectors, level by level, for arbitrary minimal models $\mathcal{M}(p', p)$. Alternatively, these could be obtained level-by-level from the null vectors of the Gram matrix for Virasoro states.

We first present our general algorithm for the Virasoro generators in the L_1 -basis. In the subsequent subsection, we implement this algorithm for generic c in the $h = 0$ vacuum sector pointing out its salient features and discuss the relation between the L_1 -basis and the basis of Virasoro states. We illustrate our algorithms for the tricritical Ising in Section 6. In each case the algorithm can be efficiently implemented using Mathematica [23].

5.1. Matrix algorithms for Virasoro generators in L_1 -basis

Because states belonging to different Virasoro modules are orthogonal, the matrices representing the Virasoro generators L_n can be obtained separately within each module \mathcal{V}_h

$$L_n = \bigoplus_h L_n^h. \tag{5.1}$$

Usually we work within a fixed module and suppress the index h . To obtain matrix representations of Vir, we will take $L_{-n} = L_n^T$. For unitary theories L_n will be real so that $L_{-n} = L_n^T = L_n^\dagger$ whereas for nonunitary theories L_n will be complex with $L_{-n} = L_n^T \neq L_n^\dagger$. Suppose we can find a diagonal matrix L_0 and matrices $L_1 = L_{-1}^T, L_2 = L_{-2}^T$ satisfying

$$\begin{aligned} [L_1, L_0] &= L_1, & [L_2, L_0] &= 2L_2, \\ [L_1, L_{-1}] &= 2L_0, & [L_2, L_{-1}] &= 3L_1, & [L_2, L_{-2}] &= 4L_0 + c/2. \end{aligned} \tag{5.2}$$

Then we can extend this to a matrix representation of the full Virasoro algebra by recursively defining

$$L_n = L_{-n}^T = \frac{1}{n-2} [L_{n-1}, L_1], \quad n \geq 3. \tag{5.3}$$

Note that, if the generators L_n satisfy the Virasoro algebra, then the generators

$$L'_n = U^T L_n U, \quad U^T = U^{-1} \tag{5.4}$$

also satisfy the Virasoro algebra where $U = \bigoplus U^h$ is orthogonal and preserves the sectors (5.1). This corresponds to the freedom of an orthogonal change of basis. To specify a unique matrix representation of the Virasoro algebra one must first specify a distinguished *canonical* basis. The generators L_{-n} act naturally on the basis (2.14) of Virasoro states. In particular, the grading of these states imposes a block structure on the matrix representatives of the Virasoro generators

$$L_{-n}^h = \bigoplus_{\ell} L_{-n,\ell}^h, \quad L_{-n,\ell}^h: \mathcal{V}_{h,\ell} \rightarrow \mathcal{V}_{h,\ell+n}. \tag{5.5}$$

The orthogonal matrix (5.4) must respect this grading so that

$$U^h = \bigoplus_{\ell=0}^{\infty} U_{\ell}^h. \tag{5.6}$$

Within $\mathcal{V}_{h,\ell}$, the Virasoro states (2.14) with $\ell = \sum_{i=1}^j n_i$ are degenerate. However, they are not orthogonal and typically they contain null vectors, so a basis of Virasoro states (2.14) is not a good basis to choose in seeking matrix representations of the Virasoro generators. One possibility, is to use the Gram–Schmidt process to orthonormalize the Virasoro states with the null vectors removed. A better alternative, at least for unitary minimal models, is to use the basis of fermion states. Since the fermion basis is a complete orthonormal basis of physical states we do not have to worry about removing null vectors. To obtain matrix representations of the Virasoro generators, we therefore start working in a fixed orthonormal basis of states.

With such a choice of basis, the structure of the matrices $L_1 = L_{-1}^T$ and $L_2 = L_{-2}^T$ is

$$L_1 = \begin{matrix} & d_0 & d_1 & d_2 & \cdots & d_{\ell-1} & & d_{\ell} \\ \begin{matrix} d_0 \\ d_1 \\ d_2 \\ \vdots \\ d_{\ell-1} \end{matrix} & \left(\begin{array}{cccccccc} \mathbf{0} & \star & \mathbf{0} & & & & & \\ & \mathbf{0} & \star & & & & & \\ & & \mathbf{0} & & & & & \\ & & & \ddots & & & & \\ & & & & & * & 0 & 0 & 0 & 0 & 0 & 0 \\ & & & & & 0 & * & 0 & 0 & 0 & 0 & 0 \\ & & & & & 0 & 0 & * & 0 & 0 & 0 & 0 \\ & & & & & 0 & 0 & 0 & * & 0 & 0 & 0 \end{array} \right) \end{matrix}, \tag{5.7}$$

$$L_2 = \begin{matrix} & d_0 & d_1 & d_2 & \cdots & d_{\ell-1} & & d_\ell \\ d_0 & \left(\begin{array}{cccccccc} \mathbf{0} & \mathbf{0} & \star & & & & & \\ & \mathbf{0} & \mathbf{0} & & & & & \\ & & \mathbf{0} & & & & & \\ & & & \ddots & & & & \\ & & & & \ddots & & & \\ & & & & & * & * & * & * & * & 0 & 0 \\ & & & & & * & * & * & * & * & * & 0 \\ & & & & & * & * & * & * & * & * & * \end{array} \right) & \\ d_1 & & & & & & & & & & & & \\ d_2 & & & & & & & & & & & & \\ \vdots & & & & & & & & & & & & \\ d_{\ell-2} & & & & & & & & & & & & \end{matrix}, \tag{5.8}$$

where $d_\ell = d_\ell^h = \dim \mathcal{V}_{h,\ell}$ as in (2.16), \star denotes nonzero off-diagonal blocks, the nonzero ℓ -blocks in position ℓ are of sizes $d_{\ell-1} \times d_\ell$ and $d_{\ell-2} \times d_\ell$ respectively and

$$\chi_h(q) = q^{-c/24+h} \sum_{\ell=0}^{\infty} d_\ell q^\ell. \tag{5.9}$$

We allow for arbitrary entries in each nonzero block, substitute into the basic Virasoro commutators (5.2) and proceed to solve the equations level-by-level. At a given level, we find that the equations are underdetermined and only involve dot products between rows in the ℓ -blocks. This freedom corresponds to an allowed change of orthogonal basis implemented by the orthogonal matrix U_ℓ^h and is removed by demanding that the entries above the leading diagonal vanish in the $(d_{\ell-1} + d_{\ell-2}) \times d_\ell$ matrix B_ℓ formed by placing the ℓ block of L_1 above the ℓ -block of L_2 . In this basis, we find that the entries below the leading diagonal of the ℓ -block of L_1 automatically vanish. There remains a residual freedom associated with the choice of sign of each of the basis elements. We remove this by further demanding that the first nonzero entry at the top of each column of B_ℓ is positive. If this is pure imaginary, as can occur in nonunitary cases, we demand that the imaginary part of this nonzero entry of B_ℓ is positive. This algorithm thus fixes a distinguished *canonical* basis which we call the L_1 -basis because of the diagonal form of the blocks of L_1 . The L_1 -basis should be viewed as the fermionic basis of paths rotated by the orthogonal transformation U . Notice that only the level degeneracies, which can be read off from the Virasoro character, and the orthonormality of the starting basis is essential in this algorithm—the precise description of the starting basis is unimportant.

5.2. Generic minimal Virasoro matrices and L_1 basis

Let us consider the minimal models $\mathcal{M}(p', p)$ with $p = L + 1$ large. It is then natural to consider fermionic paths on A_∞ and to treat the central charge c as a parameter. We will see that this case is generic in the sense that specific minimal models can be obtained by specializing c .

In the vacuum $h = 0$ sector the generic Virasoro character is

$$\chi_0(q) = \frac{q^{-c/24}(1 - q)}{\prod_{n=1}^{\infty} (1 - q^n)}$$

$$\begin{aligned}
 & 1 \quad |0\rangle \\
 & q^2 \quad \sqrt{\frac{2}{c}} L_{-2}|0\rangle \\
 & q^3 \quad \frac{1}{\sqrt{2c}} L_{-3}|0\rangle \\
 & 2q^4 \quad \frac{1}{\sqrt{5c}} L_{-4}|0\rangle \quad - \frac{\sqrt{2}(3L_{-4}-5L_{-2}^2)|0\rangle}{5\sqrt{c(c+\frac{22}{5})}} \\
 & 2q^5 \quad \frac{1}{\sqrt{10c}} L_{-5}|0\rangle \quad - \frac{(2L_{-5}-5L_{-3}L_{-2})|0\rangle}{5\sqrt{c(c+\frac{22}{5})}} \\
 & 4q^6 \quad \sqrt{\frac{2}{35c}} L_{-6}|0\rangle \quad - \frac{(8L_{-6}-10L_{-4}L_{-2}-5L_{-3}^2)|0\rangle}{15\sqrt{2c(c+\frac{22}{5})}} \\
 & \quad \frac{(20L_{-6}+56L_{-4}L_{-2}-35L_{-3}^2)|0\rangle}{42\sqrt{10c(c+\frac{29}{10})}} \quad - \frac{((78+60c)L_{-6}+(201+126c)L_{-4}L_{-2}-93L_{-3}^2-(29+70c)L_{-2}^3)|0\rangle}{35\sqrt{3c(c-\frac{1}{2})(c+\frac{22}{5})(c+\frac{68}{7})(c+\frac{29}{10})}} \\
 & 4q^7 \quad \dots \quad \dots
 \end{aligned}$$

Fig. 10. L_1 -basis of orthonormal states for the generic Virasoro module \mathcal{V}_0 in terms of Virasoro states. The central charge c is treated as a parameter. Unphysical (null) states appear if c is set to the value of the central charge of a minimal model. For the Ising model with $c = 1/2$ an unphysical state appears at level $\ell = 6$. The apparent singularity of the state is an artifact of the normalization. Actually, the numerator is a null state. Further null states appear for the nonunitary cases with $c = -22/5$ and $c = -68/7$ corresponding to $\mathcal{M}(2, 5)$ and $\mathcal{M}(2, 7)$.

zero column of L_2 at the original position 15, corresponding to the single null vector at level 7, so we remove this row and column. At the next stage we remove rows and columns at the original positions 19 and 22, corresponding to the two null vectors at level 8, and so on. This process exactly produces the Virasoro generators of the critical Ising model $\mathcal{M}(3, 4)$ as given in Section 4 of [11]. The same process works for the Yang–Lee theory with $c = -22/5$ as given in Section 7 of [11] and other special values of c corresponding to minimal models. Indeed, the matrix L_2 exhibits a remarkable structure of factors of the form $\sqrt{c - c_{p',p}}$ where $c_{p',p}$ is the central charge of the minimal model $\mathcal{M}(p', p)$.

The elements of the L_1 -basis can be obtained in terms of the Virasoro states from the generic minimal Virasoro matrices $L_{-n} = L_n^T$, $n = 1, 2$ by considering the action of these matrices on the fundamental basis formed by the column vectors $e_i = \{\delta_{i,j}\}_{j=1,2,\dots}$. We identify e_1 with the vacuum $|0\rangle$. Using the action of the Virasoro algebra on the states, the next states are identified as

$$L_{-2}e_1 \equiv L_{-2}|0\rangle = \sqrt{\frac{c}{2}} e_2 \quad \Rightarrow \quad e_2 = \sqrt{\frac{2}{c}} L_{-2}|0\rangle, \tag{5.15}$$

$$L_{-1}e_2 \equiv \sqrt{\frac{2}{c}} L_{-3}|0\rangle = 2e_3 \quad \Rightarrow \quad e_3 = \frac{1}{\sqrt{2c}} L_{-3}|0\rangle. \tag{5.16}$$

This procedure continues for higher levels leading to the expressions in Fig. 10. These expressions hold for both unitary and nonunitary models. The orthonormality of the L_1 basis is guaranteed by the orthonormality of the fundamental basis e_i .

5.3. Matrix algorithm for fields

An algorithm can similarly be applied level-by-level to obtain matrix representations of the primary fields $\phi^{(h)}(z)$. Unlike the generators L_n , a chiral primary field $\phi^{(h)}(z)$

intertwines between different Virasoro modules, its action being dictated by the fusion rules

$$\phi^{(h_i)} \times \phi^{(h_j)} = \sum_k \mathcal{N}_{ij}^k \phi^{(h_k)}. \tag{5.17}$$

If the fusion coefficient is $\mathcal{N}_{ij}^k \neq 0$ then the corresponding restriction of the field $\phi^{(h_i)}$, called chiral vertex operator (CVO), is nonzero

$$\phi \left(\begin{matrix} h_i \\ h_k, h_j \end{matrix} \right) (z): \mathcal{V}_{h_j} \rightarrow \mathcal{V}_{h_k}. \tag{5.18}$$

The CVOs admit the Laurent expansion

$$\phi \left(\begin{matrix} h \\ h_2, h_1 \end{matrix} \right) (z) = z^{h_2-h_1-h} \sum_{k \in \mathbb{Z}} \phi \left(\begin{matrix} h \\ h_2, h_1 \end{matrix} \right)_{k+h_1-h_2} z^{-k} \tag{5.19}$$

with the operator modes

$$\phi \left(\begin{matrix} h \\ h_2, h_1 \end{matrix} \right)_{k+h_1-h_2} = \oint \frac{dz}{2\pi i} z^{k-1} \phi \left(\begin{matrix} h \\ h_2, h_1 \end{matrix} \right) (z) z^{h_1+h-h_2}, \quad k \in \mathbb{Z}. \tag{5.20}$$

In the vector space $\mathcal{V}_{h_1} \oplus \mathcal{V}_{h_2}$ we consider the action of the two CVOs

$$\phi \left(\begin{matrix} h \\ h_2, h_1 \end{matrix} \right) (z): \mathcal{V}_{h_1} \rightarrow \mathcal{V}_{h_2}, \tag{5.21}$$

$$\phi \left(\begin{matrix} h \\ h_1, h_2 \end{matrix} \right) (z): \mathcal{V}_{h_2} \rightarrow \mathcal{V}_{h_1}. \tag{5.22}$$

The Virasoro generators and fields have the following block structure when acting on $\mathcal{V}_{h_1} \oplus \mathcal{V}_{h_2}$

$$L_n = \begin{pmatrix} L_n^{h_1} & \mathbf{0} \\ \mathbf{0} & L_n^{h_2} \end{pmatrix}, \quad \phi^{(h)}(z) = \begin{pmatrix} \mathbf{0} & \phi \left(\begin{matrix} h \\ h_1, h_2 \end{matrix} \right) (z) \\ \phi \left(\begin{matrix} h \\ h_2, h_1 \end{matrix} \right) (z) & \mathbf{0} \end{pmatrix}. \tag{5.23}$$

The representations of the two CVOs can be worked out separately because they do not mix under the commutation relation due to the block structure of the generators L_n . So we consider $\phi \left(\begin{matrix} h \\ h_2, h_1 \end{matrix} \right) (z)$ and expand the field in modes

$$\Phi(z) = \begin{pmatrix} \mathbf{0} & \mathbf{0} \\ \phi \left(\begin{matrix} h \\ h_2, h_1 \end{matrix} \right) (z) & \mathbf{0} \end{pmatrix}, \quad \Phi_k = \begin{pmatrix} \mathbf{0} & \mathbf{0} \\ \phi \left(\begin{matrix} h \\ h_2, h_1 \end{matrix} \right)_{k+h_1-h_2} & \mathbf{0} \end{pmatrix} \tag{5.24}$$

Working in the L_1 -basis for \mathcal{V}_{h_1} and \mathcal{V}_{h_2} , the block structure of the mode $\binom{h}{h_2, h_1}_{h_1-h_2}$ is

$$\phi \left(\binom{h}{h_2, h_1} \right)_{h_1-h_2} = \begin{pmatrix} d_0^{h_1} & d_1^{h_1} & d_2^{h_1} & \dots & d_\ell^{h_1} \\ d_0^{h_2} & \star & \mathbf{0} & & \\ d_1^{h_2} & \mathbf{0} & \star & & \mathbf{0} \\ d_2^{h_2} & \mathbf{0} & \mathbf{0} & \star & \\ \vdots & & & \ddots & \\ d_\ell^{h_2} & & & & * & * & * & * \\ & & & & * & * & * & * \\ & & & & * & * & * & * \\ & & & & * & * & * & * \\ & & & & * & * & * & * \\ & & & & * & * & * & * \\ & & & & & & \ddots & \end{pmatrix}, \tag{5.25}$$

where

$$\begin{aligned} \chi_{h_1}(q) &= q^{-c/24+h_1} \sum_{\ell=0}^{\infty} d_\ell^{h_1} q^\ell, \quad d_\ell^{h_1} \geq 0, \\ \chi_{h_2}(q) &= q^{-c/24+h_2} \sum_{\ell=0}^{\infty} d_\ell^{h_2} q^\ell, \quad d_\ell^{h_2} \geq 0. \end{aligned} \tag{5.26}$$

The primary fields satisfy

$$\delta_m \phi^{(h)}(z) = [L_m, \phi^{(h)}(z)] = z^{m+1} \frac{\partial}{\partial z} \phi^{(h)}(z) + h(m+1)z^m \phi^{(h)}(z) \tag{5.27}$$

and consequently the modes satisfy

$$\left[L_m, \phi \left(\binom{h}{h_2, h_1} \right)_{k+h_1-h_2} \right] = [-m(1-h) - (k+h_1-h_2)] \phi \left(\binom{h}{h_2, h_1} \right)_{m+k+h_1-h_2}. \tag{5.28}$$

Given the mode Φ_0 , we use this to generate the remaining modes by the action of the known matrix representation of L_n

$$\Phi_n = \frac{1}{n(h-1) + h_2 - h_1} [L_n, \Phi_0], \quad n \neq 0. \tag{5.29}$$

With the higher modes defined in this way, we solve the linear equations

$$\begin{aligned} [L_1, \Phi_1] &= (h-2+h_2-h_1)\Phi_2, & [L_1, \Phi_{-1}] &= (h+h_2-h_1)\Phi_0, \\ [L_2, \Phi_{-1}] &= (2h-1+h_2-h_1)\Phi_1 \end{aligned} \tag{5.30}$$

$$\oplus \begin{pmatrix} 11\sqrt{\frac{7}{15}} & \sqrt{\frac{119}{330}} & 2\sqrt{\frac{2}{21}} & 0 & \frac{1}{2}\sqrt{\frac{65}{231}} & 0 & 0 & 0 \\ 0 & 5\sqrt{\frac{15}{11}} & \frac{4}{13}\sqrt{51} & \frac{27}{13}\sqrt{\frac{3}{14}} & \frac{5}{13}\sqrt{\frac{255}{286}} & \frac{1}{26}\sqrt{\frac{4295}{13}} & 0 & \frac{1}{2\sqrt{105}} \\ 0 & 0 & 19\sqrt{\frac{3}{91}} & 0 & \frac{41}{13}\sqrt{\frac{66}{35}} & \frac{1}{52}\sqrt{\frac{102221}{5}} & 0 & \frac{-7}{4}\sqrt{\frac{17}{195}} \\ 0 & 0 & 0 & 19\sqrt{\frac{3}{91}} & 0 & 81\sqrt{\frac{2}{4295}} & \frac{13}{2}\sqrt{\frac{1443}{4295}} & 9\sqrt{\frac{6}{455}} \end{pmatrix} \oplus \dots \tag{6.4}$$

We thus obtain the energy–momentum tensor of the tricritical Ising model as shown in Fig. 11. As a further example of our algorithms, we also exhibit the primary field $(\frac{3}{5}, 0)(z)$ in the L_1 basis in Fig. 12.

7. Discussion

In this paper we have considered the minimal CFTs from a lattice approach. In particular, we have exhibited a bijection between the one-dimensional configuration paths and the eigenstates of the critical A_L RSOS double row transfer matrices. Our presentation here of the classification of these eigenstates and the details of the energy-preserving bijection however is incomplete. The task of extending this to all (r, s) sectors of the unitary minimal models $\mathcal{M}(L, L + 1)$ will be completed elsewhere [20]. We also hope to discuss the modifications required to treat the nonunitary models in future work.

In terms of conformal field theory we have taken steps towards the fermionization of the $sl(2)$ minimal and parafermion conformal field theories by associating orthonormal fermionic states with the paths of the underlying lattice models. In this way we are able to build the Hilbert space of physical states of these models on the cylinder in terms of lattice RSOS paths labeling the eigenstates of double-row transfer matrices. The fermionic states have the advantage over Virasoro states in that they are automatically orthonormal.

The results of this paper extend [20] to periodic and other conformal boundary conditions. In the case of periodic boundaries, there are two copies of the Virasoro algebra and the states are labeled by two RSOS paths. In the plane of the complex spectral parameter u , these come from the distinct patterns of zeros in the upper and lower half-planes corresponding respectively to the left- and right-chiral halves. Our analysis will thus put the finitized toroidal partition functions postulated by Melzer [9] on a firm footing.

In this paper we also have presented a general level-by-level algorithm to build matrix representations of the Virasoro algebra and fields for the $sl(2)$ minimal and parafermion models. We expect this algorithm to work generally for rational CFTs.

Although our algorithm appears to be consistent level-by-level, our results are far from complete. We have no proof that the infinite matrices actually give a representation of the Virasoro algebra. Although it is probably not difficult to establish the convergence of our truncated matrices to order q^N , it would be highly desirable to have closed form expressions for the infinite matrices. Likewise, it is highly desirable to obtain explicit expressions for the Virasoro generators in terms of the fermion operators. In treating the fields we have for simplicity worked with one chiral half of the bulk fields. It is possible [20] to extend this to a full treatment of the bulk fields for the periodic system but it would also be nice to give a proper treatment of the boundary fields on the cylinder.

$$T(z) = \begin{pmatrix}
 0 & \frac{1}{2z^4}\sqrt{\frac{7}{5}} & \frac{1}{z^5}\sqrt{\frac{7}{5}} & \frac{1}{z^6}\sqrt{\frac{7}{2}} & 0 & \frac{\sqrt{7}}{z^7} & 0 & \frac{7}{2z^8} & 0 & 0 & 0 & \frac{7}{z^9}\sqrt{\frac{2}{5}} & 0 & 0 & 0 \\
 \frac{1}{2}\sqrt{\frac{7}{5}} & \frac{2}{z^2} & \frac{2}{z^3} & \frac{3}{z^4}\sqrt{\frac{2}{5}} & \frac{1}{z^4}\sqrt{\frac{51}{10}} & \frac{4}{\sqrt{5}z^5} & \frac{1}{z^5}\sqrt{\frac{51}{5}} & \frac{2}{z^6}\sqrt{\frac{5}{7}} & \frac{1}{z^6}\sqrt{\frac{85}{6}} & \frac{2}{z^6}\sqrt{\frac{13}{21}} & 0 & \frac{3}{z^7}\sqrt{\frac{2}{7}} & \frac{\sqrt{17}}{z^7} & \frac{2}{z^7}\sqrt{\frac{13}{7}} & 0 \\
 \sqrt{\frac{7}{5}}z & \frac{2}{z} & \frac{3}{z^2} & \frac{\sqrt{10}}{z^3} & 0 & \frac{7}{\sqrt{5}z^4} & \frac{1}{2z^4}\sqrt{\frac{51}{5}} & \frac{18}{\sqrt{35}z^5} & \frac{2}{z^5}\sqrt{\frac{34}{15}} & \frac{-2}{z^5}\sqrt{\frac{13}{21}} & 0 & \frac{11}{\sqrt{14}z^6} & \frac{\sqrt{17}}{z^6} & -\frac{1}{z^6}\sqrt{\frac{13}{7}} & 0 \\
 \sqrt{\frac{7}{2}}z^2 & 3\sqrt{\frac{2}{5}} & \frac{\sqrt{10}}{z} & \frac{4}{z^2} & 0 & \frac{3\sqrt{2}}{z^3} & 0 & \frac{8}{z^4}\sqrt{\frac{2}{7}} & \frac{1}{2z^4}\sqrt{\frac{17}{3}} & \frac{1}{z^4}\sqrt{\frac{26}{105}} & 0 & \frac{5}{z^5}\sqrt{\frac{5}{7}} & \frac{1}{z^5}\sqrt{\frac{34}{5}} & -\frac{1}{z^5}\sqrt{\frac{26}{35}} & 0 \\
 0 & \sqrt{\frac{51}{10}} & 0 & 0 & \frac{4}{z^2} & 0 & \frac{2\sqrt{2}}{z^3} & 0 & \frac{2}{z^4} & \frac{2}{z^4}\sqrt{\frac{238}{65}} & \frac{27}{2\sqrt{65}z^4} & 0 & \frac{4}{z^5}\sqrt{\frac{2}{15}} & \frac{4}{z^5}\sqrt{\frac{238}{195}} & \frac{9}{z^5}\sqrt{\frac{3}{65}} \\
 \sqrt{7}z^3 & \frac{4z}{\sqrt{5}} & \frac{7}{\sqrt{5}} & \frac{3}{z}\sqrt{2} & 0 & \frac{5}{z^2} & 0 & \frac{2}{z^3}\sqrt{7} & 0 & 0 & 0 & \frac{9}{z^4}\sqrt{\frac{5}{14}} & \frac{1}{2z^4}\sqrt{\frac{17}{5}} & \frac{1}{z^4}\sqrt{\frac{13}{35}} & 0 \\
 0 & \sqrt{\frac{51}{5}}z & \frac{1}{2}\sqrt{\frac{51}{5}} & 0 & \frac{2\sqrt{2}}{z} & 0 & \frac{5}{z^2} & 0 & \frac{3\sqrt{2}}{z^3} & 0 & 0 & 0 & \frac{13}{\sqrt{15}z^4} & \frac{4}{z^4}\sqrt{\frac{119}{195}} & \frac{9}{z^4}\sqrt{\frac{3}{130}} \\
 \frac{7z^4}{2} & 2\sqrt{\frac{5}{7}}z^2 & \frac{18z}{\sqrt{35}} & 8\sqrt{\frac{2}{7}} & 0 & \frac{2\sqrt{7}}{z} & 0 & \frac{6}{z^2} & 0 & 0 & 0 & \frac{2\sqrt{10}}{z^3} & 0 & 0 & 0 \\
 0 & \sqrt{\frac{85}{6}}z^2 & 2\sqrt{\frac{34}{15}}z & \frac{1}{2}\sqrt{\frac{17}{3}} & 2 & 0 & \frac{3\sqrt{2}}{z} & 0 & \frac{6}{z^2} & 0 & 0 & 0 & \frac{\sqrt{30}}{z^3} & 0 & 0 \\
 0 & 2\sqrt{\frac{13}{21}}z^2 & -2\sqrt{\frac{13}{21}}z & \sqrt{\frac{26}{105}} & 2\sqrt{\frac{238}{65}} & 0 & 0 & 0 & 0 & \frac{6}{z^2} & 0 & 0 & 0 & \frac{2\sqrt{3}}{z^3} & 0 \\
 0 & 0 & 0 & 0 & \frac{27}{2\sqrt{65}} & 0 & 0 & 0 & 0 & 0 & \frac{6}{z^2} & 0 & 0 & 0 & \frac{2\sqrt{3}}{z^3} \\
 7\sqrt{\frac{2}{5}}z^5 & 3\sqrt{\frac{2}{7}}z^3 & \frac{11z^2}{\sqrt{14}} & 5\sqrt{\frac{5}{7}}z & 0 & 9\sqrt{\frac{5}{14}} & 0 & \frac{2\sqrt{10}}{z} & 0 & 0 & 0 & 0 & \frac{7}{z^2} & 0 & 0 & 0 \\
 0 & \sqrt{17}z^3 & \sqrt{17}z^2 & \sqrt{\frac{34}{5}}z & 4\sqrt{\frac{2}{15}}z & \frac{1}{2}\sqrt{\frac{17}{5}} & \frac{13}{\sqrt{15}} & 0 & \frac{\sqrt{30}}{z} & 0 & 0 & 0 & 0 & \frac{7}{z^2} & 0 & 0 \\
 0 & 2\sqrt{\frac{13}{7}}z^3 & -\sqrt{\frac{13}{7}}z^2 & -\sqrt{\frac{26}{35}}z & 4\sqrt{\frac{238}{195}}z & \sqrt{\frac{13}{35}} & 4\sqrt{\frac{119}{195}} & 0 & 0 & \frac{2\sqrt{3}}{z} & 0 & 0 & 0 & \frac{7}{z^2} & 0 & 0 \\
 0 & 0 & 0 & 0 & 9\sqrt{\frac{3}{65}}z & 0 & 9\sqrt{\frac{3}{130}} & 0 & 0 & 0 & \frac{2\sqrt{3}}{z} & 0 & 0 & 0 & 0 & \frac{7}{z^2}
 \end{pmatrix}$$

Fig. 11. Energy–momentum tensor (in the L_1 basis) of the tricritical Ising model in the vacuum $h = 0$ sector. Notice that the squares of the coefficients in the first column give the expansion of $(1 - u)^{-4}$ in agreement with the two-point function.

$$\phi_{(3/5, 0)}(z) = \begin{pmatrix} 1 & \frac{6}{\sqrt{35}z^2} & \frac{6}{\sqrt{35}z^3} & \frac{9}{5z^4}\sqrt{\frac{2}{7}} & \frac{8}{5z^4}\sqrt{\frac{6}{119}} & \frac{12}{5\sqrt{7}z^5} \\ \sqrt{\frac{6}{5}}z & \frac{-4\sqrt{\frac{6}{7}}}{5z} & \frac{\sqrt{\frac{6}{7}}}{5z^2} & \frac{8\sqrt{\frac{3}{35}}}{5z^3} & \frac{-16\sqrt{\frac{7}{85}}}{5z^3} & \frac{\sqrt{\frac{42}{5}}}{5z^4} \\ \frac{\sqrt{33}z^2}{5} & \frac{-4\sqrt{\frac{3}{385}}}{5} & \frac{-4\sqrt{\frac{33}{35}}}{5z} & \frac{-\sqrt{\frac{66}{7}}}{25z^2} & \frac{72\sqrt{\frac{14}{187}}}{25z^2} & \frac{2\sqrt{\frac{33}{7}}}{25z^3} \\ 0 & \frac{\sqrt{\frac{65}{77}}}{\sqrt{77}} & 0 & 0 & 0 & 0 \\ \frac{4\sqrt{\frac{11}{5}}z^3}{5} & \frac{-6z}{25\sqrt{77}} & \frac{-3\sqrt{\frac{7}{11}}}{25} & \frac{-24\sqrt{\frac{22}{35}}}{25z} & \frac{-24\sqrt{\frac{42}{935}}}{25z} & \frac{-12\sqrt{\frac{11}{35}}}{25z^2} \\ 0 & 3\sqrt{\frac{2}{77}}z & 5\sqrt{\frac{2}{77}} & 0 & \frac{-8\sqrt{\frac{3}{6545}}}{z} & 0 \\ \frac{2\sqrt{231}z^4}{25} & \frac{-\sqrt{\frac{33}{5}}z^2}{175} & \frac{-31\sqrt{\frac{3}{55}}z}{175} & \frac{-263\sqrt{\frac{2}{22}}}{875} & \frac{-12\sqrt{\frac{2}{187}}}{125} & \frac{-16\sqrt{\frac{33}{125z}}}{125z} \\ 0 & 3\sqrt{\frac{11}{1085}}z^2 & 12\sqrt{\frac{5}{2387}}z & 25\sqrt{\frac{2}{2387}} & \frac{-4\sqrt{\frac{6}{40579}}}{5} & 0 \\ 0 & \frac{3\sqrt{\frac{183}{31}}z^2}{7} & \frac{-3\sqrt{\frac{183}{31}}z}{7} & \frac{3\sqrt{\frac{183}{310}}}{7} & -148\sqrt{\frac{2}{160735}} & 0 \\ 0 & 0 & 0 & 0 & 5\sqrt{\frac{299}{7259}} & 0 \\ \frac{2\sqrt{6006}z^5}{125} & \frac{-8\sqrt{\frac{66}{875}}z^3}{875} & \frac{-41\sqrt{\frac{33}{130}}z^2}{875} & \frac{-1564\sqrt{\frac{3}{143}}z}{4375} & \frac{-72z}{625\sqrt{2431}} & \frac{-5177\sqrt{\frac{3}{286}}}{4375} \\ 0 & \frac{8\sqrt{\frac{11}{651}}z^3}{5} & \frac{\sqrt{\frac{33}{217}}z^2}{\sqrt{217}} & 5\sqrt{\frac{30}{2387}}z & \frac{-4\sqrt{\frac{2}{202895}}z}{5} & 25\sqrt{\frac{5}{7161}} \\ 0 & \frac{24\sqrt{\frac{366}{3565}}z^3}{7} & \frac{-3\sqrt{\frac{183}{7130}}z^2}{7} & \frac{-66\sqrt{\frac{183}{713}}z}{35} & \frac{-888z}{5\sqrt{739381}} & \frac{9\sqrt{\frac{183}{1426}}}{7} \\ 0 & 0 & 0 & 0 & 3\sqrt{\frac{130}{7259}}z & 0 \\ 0 & 4\sqrt{\frac{5}{897}}z^3 & -2\sqrt{\frac{15}{299}}z^2 & 2\sqrt{\frac{6}{299}}z & -2\sqrt{\frac{34}{299}}z & \frac{-2}{\sqrt{897}} \\ \frac{2\sqrt{31031}z^6}{125} & \frac{-24\sqrt{\frac{11}{403}}z^4}{625} & \frac{-408\sqrt{\frac{11}{403}}z^3}{4375} & \frac{-2589\sqrt{\frac{11}{4030}}z^2}{4375} & \frac{-12\sqrt{\frac{66}{34255}}z^2}{625} & \frac{-38991z}{4375\sqrt{22165}} \\ 0 & \frac{4\sqrt{\frac{231}{6355}}z^4}{5} & 32\sqrt{\frac{11}{133455}}z^3 & 5\sqrt{\frac{66}{8897}}z^2 & \frac{-2\sqrt{\frac{22}{151249}}z^2}{25} & 100\sqrt{\frac{3}{97867}}z \\ 0 & \frac{72\sqrt{\frac{61}{12121}}z^4}{5} & \frac{216\sqrt{\frac{61}{12121}}z^3}{35} & \frac{-801\sqrt{\frac{61}{121210}}z^2}{35} & \frac{-1628\sqrt{\frac{6}{217465}}z^2}{85} & \frac{-171\sqrt{\frac{61}{60605}}z}{7} \\ 0 & 0 & 0 & 0 & \frac{11\sqrt{\frac{39}{427}}z^2}{17} & 0 \\ 0 & \frac{\sqrt{\frac{42}{299}}z^4}{\sqrt{299}} & -2\sqrt{\frac{14}{897}}z^3 & -2\sqrt{\frac{21}{1495}}z^2 & -11\sqrt{\frac{17}{10465}}z^2 & 2\sqrt{\frac{42}{1495}}z \\ 0 & \frac{\sqrt{\frac{34698}{151249}}z^4}{\sqrt{151249}} & -2\sqrt{\frac{34698}{151249}}z^3 & 6\sqrt{\frac{17349}{756245}}z^2 & \frac{99003z^2}{17\sqrt{257256755}} & -2\sqrt{\frac{34698}{756245}}z \\ 0 & 0 & 0 & 0 & \frac{16\sqrt{4485}}{17\sqrt{40481}}z^2 & 0 \end{pmatrix}$$

Fig. 12. Primary field $\phi_{(3/5, 0)}(z)$ (in the L_1 basis) of the tricritical Ising model. The squares of the first column entries agree with $(1 - u)^{-6/5}$. (See next page.)

$\frac{16}{5z^5} \sqrt{\frac{3}{119}}$	$\frac{6}{7z^6}$	$\frac{8}{z^6} \sqrt{\frac{2}{357}}$	$\frac{47}{35\sqrt{195}z^6}$	$\frac{4}{5z^6} \sqrt{\frac{14}{3315}}$
$\frac{-72\sqrt{\frac{2}{595}}}{5z^4}$	$\frac{4\sqrt{\frac{6}{5}}}{7z^5}$	$\frac{-16}{\sqrt{595}z^5}$	$\frac{-188\sqrt{\frac{2}{13}}}{175z^5}$	$\frac{-32\sqrt{\frac{7}{221}}}{25z^5}$
$\frac{-16\sqrt{\frac{7}{187}}}{25z^3}$	$\frac{2\sqrt{33}}{35z^4}$	$\frac{-64\sqrt{\frac{2}{1309}}}{5z^4}$	$\frac{3572}{175\sqrt{715}z^4}$	$\frac{304\sqrt{\frac{14}{12155}}}{25z^4}$
$\frac{2\sqrt{\frac{39}{1309}}}{z^3}$	0	$\frac{\sqrt{\frac{78}{1309}}}{z^4}$	$\frac{2\sqrt{\frac{3}{55}}}{z^4}$	$\frac{-16\sqrt{\frac{6}{6545}}}{z^4}$
$\frac{12\sqrt{\frac{231}{85}}}{25z^2}$	0	$\frac{4\sqrt{\frac{14}{2805}}}{z^3}$	$\frac{-1786}{125\sqrt{429}z^3}$	$\frac{-1064\sqrt{\frac{14}{7293}}}{125z^3}$
$\frac{\sqrt{\frac{66}{595}}}{z^2}$	0	$\frac{16\sqrt{\frac{3}{6545}}}{z^3}$	$\frac{-14\sqrt{\frac{6}{143}}}{5z^3}$	$\frac{32\sqrt{\frac{21}{2431}}}{5z^3}$
$\frac{-504}{125\sqrt{187}z}$	$\frac{-4\sqrt{\frac{33}{7}}}{25z^2}$	$\frac{168\sqrt{\frac{2}{187}}}{25z^2}$	$\frac{2679}{125\sqrt{5005}z^2}$	$\frac{1596\sqrt{\frac{2}{12155}}}{125z^2}$
$\frac{-4\sqrt{\frac{93}{1309}}}{5z}$	0	$\frac{3\sqrt{\frac{186}{1309}}}{5z^2}$	$\frac{126\sqrt{\frac{3}{22165}}}{5z^2}$	$\frac{-144\sqrt{\frac{42}{376805}}}{5z^2}$
0	0	0	$\frac{9\sqrt{\frac{61}{2821}}}{5z^2}$	$\frac{-1652\sqrt{\frac{2}{417911}}}{15z^2}$
0	0	0	0	$\frac{26\sqrt{\frac{115}{7259}}}{3z^2}$
$\frac{-372\sqrt{\frac{2}{2431}}}{625}$	$\frac{-8\sqrt{\frac{858}{7}}}{125z}$	$\frac{-168\sqrt{\frac{13}{187}}}{125z}$	$\frac{-5358\sqrt{\frac{2}{385}}}{8125z}$	$\frac{-6384}{8125\sqrt{935}z}$
$\frac{-2\sqrt{\frac{17}{11935}}}{5}$	0	$\frac{-12\sqrt{\frac{62}{6545}}}{5z}$	$\frac{-84}{25\sqrt{4433}z}$	$\frac{96\sqrt{\frac{14}{75361}}}{25z}$
$-296\sqrt{\frac{2}{739381}}$	0	0	$\frac{-18\sqrt{\frac{122}{324415}}}{5z}$	$\frac{6608}{15\sqrt{48059765}z}$
$10\sqrt{\frac{65}{7259}}$	0	0	0	$\frac{-52\sqrt{\frac{2}{7259}}}{3z}$
$\frac{\sqrt{17}}{299}$	0	0	$\frac{-24\sqrt{\frac{7}{115}}}{13z}$	$\frac{504\sqrt{\frac{2}{1955}}}{13z}$
$\frac{-984\sqrt{\frac{3}{376805}z}}{625}$	$\frac{-903\sqrt{\frac{7}{22165}}}{125}$	$\frac{-736\sqrt{\frac{6}{376805}}}{125}$	$\frac{-1786\sqrt{\frac{3}{2387}}}{40625}$	$\frac{-1064\sqrt{\frac{6}{5797}}}{40625}$
$\frac{-142z}{25\sqrt{1663739}}$	$\frac{125}{\sqrt{41943}}$	$\frac{-63\sqrt{\frac{14}{237677}}}{25}$	$\frac{-42}{25\sqrt{908765}}$	$\frac{48\sqrt{\frac{14}{15449005}}}{25}$
$\frac{-1184\sqrt{\frac{3}{217465}z}}{17}$	$9\sqrt{\frac{305}{84847}}$	$\frac{-296\sqrt{\frac{30}{43493}}}{17}$	$\frac{-6\sqrt{\frac{183}{1103011}}}{25}$	$\frac{3304\sqrt{\frac{2}{1696227}}}{1275}$
$\frac{20\sqrt{\frac{78}{427}z}}{17}$	0	$\frac{50\sqrt{\frac{39}{427}}}{17}$	0	$\frac{-52}{51\sqrt{6405}}$
$-17\sqrt{\frac{17}{20930}z}$	$-\sqrt{\frac{10}{897}}$	$\frac{3\sqrt{\frac{85}{2093}}}{2}$	$\frac{-6\sqrt{\frac{2}{23}}}{65}$	$\frac{36\sqrt{\frac{7}{391}}}{65}$
$\frac{-99003z}{17\sqrt{514513510}}$	$\frac{\sqrt{\frac{34698}{108035}}}{7}$	$\frac{33001}{34\sqrt{257256755}}$	$\frac{-592642\sqrt{\frac{2}{1624392653}}}{35}$	$\frac{-80468\sqrt{\frac{7}{95552509}}}{85}$
$\frac{-8\sqrt{\frac{8970}{40481}z}}{17}$	0	$\frac{8\sqrt{\frac{1495}{121443}}}{17}$	$4\sqrt{\frac{782}{17349}}$	$\frac{407\sqrt{\frac{23}{121443}}}{17}$

Fig. 12. (Continued).

Lastly, in the case of the tricritical Ising and 3-state Potts models, there are extended chiral algebras, namely, the superconformal algebra and W_3 algebra. It would be nice to work out, at least level-by-level, the matrix representatives of the generators of these higher symmetry algebras.

Acknowledgements

This research is supported by the Australian Research Council. We thank Omar Foda, Vladimir Rittenberg and Ole Warnaar for discussions and Jean-Bernard Zuber for comments on the manuscript.

References

- [1] A.A. Belavin, A.M. Polyakov, A.B. Zamolodchikov, Nucl. Phys. B 241 (1984) 333–380.
- [2] P. Di Francesco, P. Mathieu, D. Sénéchal, Conformal Field Theory, Springer, 1996.
- [3] R.J. Baxter, Exactly Solved Models in Statistical Mechanics, Academic Press, London, 1982.
- [4] G.E. Andrews, R.J. Baxter, P.J. Forrester, J. Stat. Phys. 35 (1984) 193–266;
P.J. Forrester, R.J. Baxter, J. Stat. Phys. 38 (1985) 435–472.
- [5] S. Dasmahapatra, R. Kedem, T.R. Klassen, B.M. McCoy, E. Melzer, Int. J. Mod. Phys. B 7 (1993) 3617–3648;
R. Kedem, T.R. Klassen, B.M. McCoy, E. Melzer, Phys. Lett. B 304 (1993) 263–270;
R. Kedem, T.R. Klassen, B.M. McCoy, E. Melzer, Phys. Lett. B 307 (1993) 68–76.
- [6] F.D.M. Haldane, Z.N.C. Ha, J.C. Talstra, D. Bernard, V. Pasquier, Phys. Rev. Lett. 69 (1992) 2021;
D. Bernard, V. Pasquier, D. Serban, Nucl. Phys. B 428 (1994) 612–628;
P. Bouwknegt, A.W.W. Ludwig, K. Schoutens, Phys. Lett. B 359 (1995) 304–312;
P. Bouwknegt, K. Schoutens, Nucl. Phys. B 547 (1999) 501–537;
P. Bouwknegt, L. Chim, D. Ridout, Nucl. Phys. B 572 (2000) 547–573.
- [7] G. Hatayama, A. Kuniba, M. Okado, T. Takagi, Z. Tsuboi, Progr. Math. Phys. 23 (2002) 72–205;
G. Hatayama, A. Kuniba, M. Okado, T. Takagi, Z. Tsuboi, in: M. Kashiwara, T. Miwa (Eds.), MathPhys Odyssey, 2001.
- [8] M. Jimbo, T. Tiwa, Algebraic Analysis of Solvable Lattice Models, in: CBMS, Vol. 85, American Mathematical Society, 1994.
- [9] E. Melzer, Int. J. Mod. Phys. A 9 (1994) 1115–1136.
- [10] S.O. Warnaar, J. Stat. Phys. 82 (1996) 657–685;
S.O. Warnaar, J. Stat. Phys. 84 (1996) 49–83.
- [11] G. Feverati, P.A. Pearce, hep-th/0211185;
G. Feverati, P.A. Pearce, hep-th/0211186.
- [12] R.E. Behrend, P.A. Pearce, D.L. O’Brien, J. Stat. Phys. 84 (1996) 1–48.
- [13] R.E. Behrend, P.A. Pearce, J. Stat. Phys. 102 (2001) 577–640;
C. Mercat, P.A. Pearce, J. Phys. A 34 (2001) 5751–5771.
- [14] A.B. Zamolodchikov, V.A. Fateev, Sov. Phys. JEPT 62 (1985) 215–225.
- [15] R.J. Baxter, J. Phys. A 13 (1980) L61–L70.
- [16] B.L. Feigin, T. Nakanishi, H. Ooguri, Int. J. Mod. Phys. A (Suppl. 1A) 7 (1992) 217–238.
- [17] S. Dasmahapatra, O. Foda, Int. J. Mod. Phys. A 13 (1998) 501–522.
- [18] D.L. O’Brien, P.A. Pearce, S.O. Warnaar, Physica A 228 (1996) 63–77;
D.L. O’Brien, P.A. Pearce, S.O. Warnaar, Nucl. Phys. B 501 (1997) 773–799.
- [19] A. Berkovich, Nucl. Phys. B 431 (1994) 315–348.
- [20] G. Feverati, P.A. Pearce, in preparation, 2002.
- [21] M. Rösgen, R. Varnhagen, Phys. Lett. B 350 (1995) 203–211.
- [22] W.M. Koo, H. Saleur, Nucl. Phys. B 426 (1994) 459–504.
- [23] Mathematica is a Copyright of Wolfram Research, Inc., 1988–2002.